© 2022. Published by The Company of Biologists Ltd | Development (2022) 149, dev200426. doi:10.1242/dev.200426

RESEARCH ARTICLE

Orb-dependent polyadenylation contributes to PLP expression and centrosome scaffold assembly

Junnan Fang and Dorothy A. Lerit*

ABSTRACT

As the microtubule-organizing centers of most cells, centrosomes engineer the bipolar mitotic spindle required for error-free mitosis. *Drosophila* Pericentrin-like protein (PLP) directs formation of a pericentriolar material (PCM) scaffold required for PCM organization and microtubule-organizing center function. Here, we investigate the post-transcriptional regulation of *Plp* mRNA. We identify conserved binding sites for cytoplasmic polyadenylation element binding (CPEB) proteins within the *Plp* 3′-untranslated region and examine the role of the CPEB ortholog Oo18 RNA-binding protein (Orb) in *Plp* mRNA regulation. Our data show that Orb interacts biochemically with *Plp* mRNA to promote polyadenylation and PLP protein expression. Loss of *orb*, but not *orb2*, diminishes PLP levels in embryonic extracts. Consequently, PLP localization to centrosomes and its function in PCM scaffolding are compromised in *orb* mutant embryos, resulting in genomic instability and embryonic lethality. Moreover, we find that PLP overexpression restores centrosome scaffolding and rescues the cell division defects caused by *orb* depletion. Our data suggest that Orb modulates PLP expression at the level of *Plp* mRNA polyadenylation and demonstrates that the post-transcriptional regulation of core, conserved centrosomal mRNAs is crucial for centrosome function.

KEY WORDS: Centrosome, PCM, CPEB, Post-transcriptional regulation, Polyadenylation, RNA localization

INTRODUCTION

Centrosomes are microtubule-organizing centers that function in spindle assembly during cell division, cilia and flagella formation, and intracellular trafficking (Vertii et al., 2016). The centrosome comprises a pair of centrioles embedded in pericentriolar material (PCM), a matrix of proteins that directs microtubule nucleation and organization (Palazzo et al., 1999). Centrosome function relies on cell cycle-dependent oscillations in PCM recruitment before mitotic onset, followed by PCM shedding at mitotic exit (Gould and Borisy, 1977; Khodjakov and Rieder, 1999). The mechanisms that regulate oscillations in centrosome activity remain incompletely understood.

In humans, PCM recruitment and microtubule organization is supported by pericentrin (PCNT) (Dictenberg et al., 1998; Zimmerman et al., 2004; Haren et al., 2009; Lee and Rhee, 2011; Chen et al., 2014; Kim et al., 2015). Consequently, deregulation of *PCNT* is associated with severe human genetic disorders, such as Down syndrome (also known as trisomy 21) and microcephalic osteodysplastic primordial dwarfism type II (MOPD II) (Jurczyk et al., 2004; Rauch et al., 2008; Delaval and Doxsey, 2010; Galati et al., 2018). Specifically, elevated levels of PCNT underlie the ciliary defects in trisomy 21-derived fibroblasts (Galati et al., 2018). Understanding how *PCNT* expression is regulated in healthy tissues and deregulated in developmental disorders remains a critical challenge.

In *Drosophila*, Pericentrin-like protein (PLP) is the ortholog of *PCNT* (Martinez-Campos et al., 2004) with conserved roles in PCM recruitment and scaffolding and microtubule organization (Dobbelaere et al., 2008; Lerit and Rusan, 2013; Galletta et al., 2014; Lerit et al., 2015; Richens et al., 2015; Roque et al., 2018; Galletta et al., 2020). Additionally, the spatial configuration of PCNT and PLP at centrosomes is identical, with their C termini proximal to centrioles and N termini extended into the PCM (Fu and Glover, 2012; Lawo et al., 2012; Mennella et al., 2012; Sonnen et al., 2012). Intriguingly, aspects of *PCNT* and *Plp* mRNA post-transcriptional regulation are also conserved, as both *PCNT* and *Plp* mRNAs localize to centrosomes (Lécuyer et al., 2007; Sepulveda et al., 2018; Chouaib et al., 2020; Ryder et al., 2020; Safieddine et al., 2021). Therefore, the study of *Drosophila* PLP will be valuable for improving our understanding of centrosome regulation as well as providing potential insights into the mechanisms of human disease linked to *PCNT* dysfunction.

How and why *PCNT* or *Plp* mRNAs localize to the centrosome is largely unknown, although recent work implicates a co-translational transport mechanism (Sepulveda et al., 2018; Chouaib et al., 2020; Safieddine et al., 2021). RNA localization coupled with translational control is a conserved regulatory paradigm used to generate spatial enrichments in gene activity and is essential for diverse cellular processes (reviewed by Cody et al., 2013; Buxbaum et al., 2015; Ryder and Lerit, 2018). RNA localization and translational control are often regulated by RNA-binding proteins (RBPs), which recognize *cis*-elements within the 3′-untranslated regions (UTRs) of target RNAs (Kislauskis et al., 1994).

One conserved family of RBPs implicated in RNA localization and translational control is the cytoplasmic polyadenylation element binding (CPEB) protein family (Mendez and Richter, 2001). CPEB proteins bind to target mRNAs through recognition of cytoplasmic polyadenylation element (CPE) motifs and promote mRNA polyadenylation following phosphorylation by Aurora A kinase (Mendez et al., 2000a; Mendez et al., 2000b; Hodgman et al., 2001). CPEB proteins promote the translation of some mRNA targets, such as *c-mos* (*mos*), *p53*, *cyclin B1* and *β-casein* (*Csn2*) mRNAs (Stebbins-Boaz et al., 1996; Groisman et al., 2000; Mendez et al., 2000b; Cao and Richter, 2002; Choi et al., 2004; Burns and Richter, 2008; Burns et al., 2011), but represses the translation of others, including *myc* mRNA (Groisman et al., 2006). Furthermore, CPEB can mediate localization of its target mRNAs independently of its

Department of Cell Biology, Emory University School of Medicine, Atlanta, GA 30322, USA.

*Author for correspondence (dlerit@emory.edu)

J.F., 0000-0002-8534-0498; D.A.L., 0000-0002-3362-8078

Handling Editor: Thomas Lecuit
Received 2 December 2021; Accepted 25 May 2022

Development (2022) 149, dev200426. doi:10.1242/dev.200426

polyadenylation or translation activities, as shown with zonal occludens-1 (*Tjp1*) mRNA (Nagaoka et al., 2012).

Drosophila encodes two CPEB proteins, Oo18 RNA-binding protein (Orb) and Orb2 (Lantz et al., 1992; Hafer et al., 2011). Whereas Orb2 functions are best defined in the testis and central nervous system (Keleman et al., 2007; Mastushita-Sakai et al., 2010; Hafer et al., 2011; Xu et al., 2012), Orb regulates RNA localization and translation during oogenesis and early embryogenesis (Lantz et al., 1992; Christerson and McKearin, 1994; Chang et al., 2001; Castagnetti and Ephrussi, 2003; Rojas-Ríos et al., 2015). Orb is orthologous to mammalian CPEB1 and similarly promotes polyadenylation to regulate the stability and translation of its target mRNAs, including *oskar* (*osk*), *gurken* (*grk*), and *Autophagy-related 12* (*Atg12*) mRNAs (Christerson and McKearin, 1994; Chang et al., 1999, 2001; Castagnetti and Ephrussi, 2003; Norvell et al., 2015; Rojas-Ríos et al., 2015; Davidson et al., 2016).

Recent transcriptomics identified numerous mRNA targets of Orb from *Drosophila* S2 cells and of CPEB1 from cultured mammalian cells (Stepien et al., 2016; Pascual et al., 2021). Among the Orb/CPEB1 mRNA targets are several mRNAs encoding centrosome proteins. In *Xenopus* and cultured mammalian cells, CPEB proteins also localize to centrosomes, and mRNAs localizing to spindle poles show enrichment of CPE motifs in their 3′-UTRs (Groisman et al., 2000; Blower et al., 2007; Eliscovich et al., 2008; Sharp et al., 2011; Pascual et al., 2021). These data are consistent with a model whereby CPEB proteins regulate components of the mitotic machinery. However, whether Orb contributes to the post-transcriptional regulation of centrosomal mRNAs remains to be investigated.

In this study, we analyzed the common mRNA targets of human CPEB1 and *Drosophila* Orb and identified *PCNT*/*Plp* mRNA. To test a role for Orb in regulating *Plp* mRNA, we identified a specific biochemical association between Orb and *Plp* mRNA and examined the role of Orb in *Plp* mRNA localization to centrosomes and translational control. Although dispensable for *Plp* mRNA localization, Orb specifically regulates PLP protein expression by promoting polyadenylation of the short *Plp* 3′-UTR. We demonstrate that Orb contributes to PLP protein localization and PCM organization at centrosomes, which is required for genome stability. Our data suggest that *Plp* mRNA is a crucial target of Orb that is required for embryonic viability and highlight the translational regulation of centrosomal mRNAs as important for centrosome activity and function.

RESULTS

Plp mRNA localizes at centrosomes during early embryogenesis

During the first 2 h of development, the *Drosophila* embryo develops as a syncytium wherein the somatic nuclei rapidly divide through abridged (S-M) mitotic cycles and migrate to the embryonic cortex prior to cellularization during nuclear cycle (NC) 14 (Rothwell and Sullivan, 1999). We recently reported that multiple mRNAs encoding proteins required for centrosome function, including *Plp* mRNA, localize to embryonic centrosomes in a cell cycle-dependent manner (Ryder et al., 2020). To analyze further how *Plp* mRNA localization to the centrosome is regulated by cell cycle progression, we performed single-molecule fluorescence *in situ* hybridization (smFISH) for *Plp* mRNA and a control transcript, *Gapdh1* mRNA, throughout syncytial development and quantified mRNA distributions relative to centrosomes labeled with GFP-γ-Tubulin (GFP-γTub). Despite relatively fewer smFISH signals, consistent with lower levels of *Plp* mRNA expression relative to *Gapdh1* (Graveley et al., 2011), some molecules of *Plp* mRNA overlapped with centrosomes (Fig. 1A,B, arrowheads). In contrast, *Gapdh1* mRNA was dispersed throughout the cytoplasm and fewer molecules overlapped with centrosomes (Fig. 1C,D).

To compare the distributions of *Plp* versus *Gapdh1* mRNAs quantitatively, we measured the percentage of mRNA overlapping centrosomes (0 µm away) using a custom Python package (Ryder et al., 2020; Ryder and Lerit, 2020). From this analysis, we observed significantly more *Plp* mRNA localized to centrosomes relative to *Gapdh1* mRNA (3∼8-fold more *Plp* mRNA than *Gapdh1* mRNA at interphase versus 2∼6-fold more at metaphase; Fig. 1E, Table S1). As the syncytial embryo undergoes successive nuclear divisions, the size of each pseudo-cell becomes progressively smaller (Foe and Alberts, 1983). Consequently, the percentage of mRNA residing near centrosomes increases with each NC. Nonetheless, *Plp* mRNA remained significantly enriched at centrosomes relative to *Gapdh1* throughout syncytial development, particularly during interphase. Although the higher-expressing *Gapdh1* mRNA showed less enrichment at centrosomes than *Plp* mRNA, it remains a formal possibility the overlap of *Plp* mRNA signals with centrosomes arises through spurious coincidence of red and green pixels. To test for spurious overlap, we compared *Plp* and *Gapdh1* mRNA localization to the centrosome from NC 13 interphase images before and after rotating the RNA channel by 90°. Significantly less *Plp* mRNA overlapped with centrosomes after rotation, to a similar level as *Gapdh1* mRNA. In contrast, *Gapdh1* mRNA distributions remained unchanged following rotation (Fig. 1F). These data verify the specific and significant enrichment of *Plp* mRNA at centrosomes. Furthermore, imaging of *Plp* mRNA together with a *GFP-PLP* transgene revealed that *Plp* mRNA and protein partially overlap at centrosomes (Fig. 1G), as recently detected in cultured mammalian cells (Sepulveda et al., 2018; Safieddine et al., 2021). Taken together, we conclude that *Plp* mRNA localizes to centrosomes, likely via a dynamic process that may involve translational control.

Plp mRNA associates with Orb protein

RNA localization coupled with translational control is a conserved mechanism that functions in various cellular contexts and is commonly regulated by RBPs (reviewed by Buxbaum et al., 2015; Das et al., 2021). Transcriptomics has uncovered thousands of predicted direct mRNA targets of Orb and Orb2 in *Drosophila* S2 cells (Stepien et al., 2016). Analysis in HeLa cells also uncovered thousands of putative mRNA targets of orthologous CPEB1 and CPEB4 (Pascual et al., 2021). We compared the RNA substrates of homologous Orb and CPEB1 proteins (Hake and Richter, 1994) identified in the Stepien and Pascual datasets and found 195 common genes (Fig. 2A; Table S2). Analysis of the gene ontologies within the common genes using the cellular component function in PANTHER uncovered significantly enriched ontologies related to the centrosome, as represented by *PCNT/Plp*, *CEP192/spd-2* and *PLK1/polo* mRNAs (Fig. S1, Table S2) (Mi et al., 2021). In accordance, recent work shows that CPEB1 is required for the translation and recruitment of Polo-like kinase (PLK1) to centrosomes (Pascual et al., 2021). Here, we focused our subsequent analysis on PLP.

Most Orb targets contain a CPE consensus motif (e.g. UUUUAU/U or UUUUAAU) in their 3′-UTR (Fox et al., 1989; McGrew and Richter, 1990; Stepien et al., 2016), although CPEB proteins can also recognize non-canonical CPE motifs [e.g. UUUUACU or UUUUAAGU (Piqué et al., 2008) or UUUUAA (Barkoff et al., 2000) or UUUUGU (Stepien et al., 2016)]. As a first step of validating *Plp* mRNA as an Orb target, we identified two consensus CPE motifs within the *Plp* 3′UTR (Fig. 2B, red boxes).

Development (2022) 149, dev200426. doi:10.1242/dev.200426

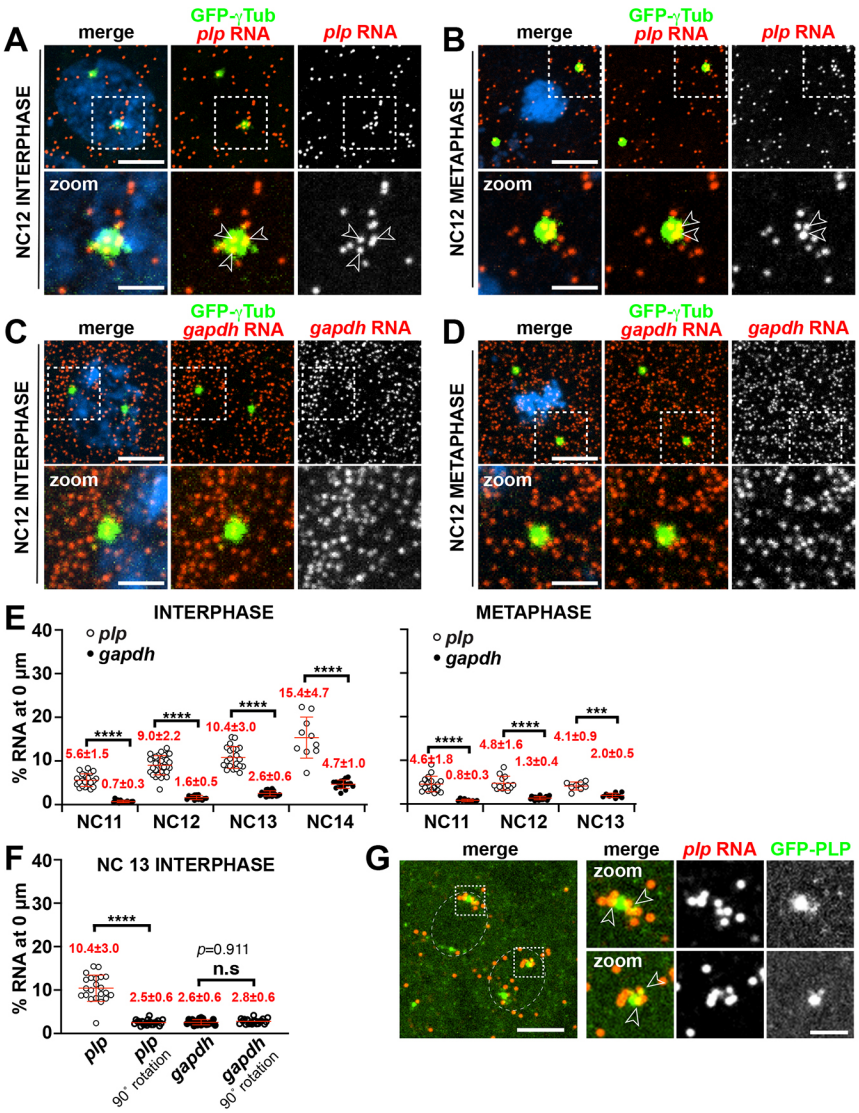

Fig. 1. *Plp* mRNA localizes to centrosomes. (A-D) Maximum intensity projections of NC 12 control embryos expressing *GFP-γTub* (green) labeled with *Plp* smFISH probes (red) in interphase (A) and metaphase (B) or *Gapdh1* smFISH probes (red) in interphase (C) and metaphase (D). Boxed regions are enlarged below. Arrowheads mark mRNA overlapping with centrosomes. (E) Quantification of *Plp* versus *Gapdh1* mRNA localization to centrosomes at different NC stages. Table S1 lists the number of embryos, centrosomes and RNA objects quantified per condition. (F) Quantification of RNA localization to centrosomes in NC 13 interphase embryos reproduced from (E) then re-measured following 90° rotation of the RNA channel. (G) NC 13 *Drosophila* embryo expressing *GFP-PLP* (green) and labeled with *Plp* smFISH probes (red). Dashed ovals mark the pseudo-cells, and insets show *Plp* mRNA overlapping PLP protein (arrowheads). Mean±s.d. are displayed. n.s., not significant; ***P<0.001; ****P<0.0001 by one-way ANOVA followed by Dunnett's T3 multiple comparisons test. Scale bars: 5 µm (main panels); 1 µm (insets).

Next, we aligned the *Plp* 3′-UTR across multiple *Drosophila* species using the conservation insect track on the UCSC genome browser and found that these CPE motifs were conserved across millions of years of evolutionary distance (Fig. 2B; Kent et al., 2002). Finally, we aligned *Drosophila melanogaster Plp* and human *PCNT* 3′UTRs using Clustal Omega (Madeira et al., 2019). *Plp* transcripts utilize one of two different 3′-UTRs varying in length: a short 3′-UTR (431 nt) or a long 3′-UTR (591 nt) (Graveley et al., 2011). The short *Plp* 3′-UTR has 100% identity with the long *Plp* 3′-UTR and 44.6% identity with the *PCNT* 3′-UTR, whereas the long *Plp* 3′-UTR has 46.9% identity with the *PCNT* 3′-UTR. All three 3′-UTRs contain two consensus CPE motifs (Fig. 2B, red boxes). Conservation of CPE sites within the *Plp* 3′UTR indicates that they are likely to be biologically relevant.

The context of CPE sites is also important for their function. To support formation of the polyadenylation complex, CPE sites are typically situated within 100 nt from the hexanucleotide AAUAAA motif recognized by the cleavage and polyadenylation specificity factor (CPSF) complex (Mendez et al., 2000b). The second CPE motif located within the *Plp* 3′UTR is proximal to a CPSF motif (Fig. 2B, green boxes), suggestive of a role in translational control.

To investigate whether Orb associates with *Plp* mRNA during early development, we used a GFP-Orb gene trap, which inserts *gfp* coding sequences at the endogenous *orb* locus (Nagarkar-Jaiswal et al., 2015), to affinity purify interacting mRNAs by RT-PCR. Similar to endogenous *orb* expression, we detected GFP-Orb more readily in ovaries compared with embryos (Lantz et al., 1992, 1994; Rangan et al., 2009; Hafer et al., 2011) (Fig. S2A,B). Using GFP-Orb ovarian extracts, we confirmed that Orb associates with *orb* mRNA, consistent with prior work (Tan et al., 2001), which also demonstrates that the Orb fusion protein is competent to bind mRNA targets (Fig. 2C). We also detected a ∼7.5-fold enrichment of *Plp* mRNA in GFP-Orb immunoprecipitated samples over the WT control. In contrast, the negative control, *Gapdh1* mRNA, was not pulled down (Fig. 2C). We conclude that *Plp* mRNA associates biochemically with Orb during early development.

Orb is dispensable for *Plp* mRNA localization

To examine whether Orb contributes to *Plp* mRNA localization to centrosomes, we compared *Plp* mRNA distributions using smFISH in control versus *orb* mutant embryos. To examine maternal effects, we harvested embryos from transheterozygous orb^{F343}/orb^{mel} (hereafter, *orb*) mutant mothers. Whereas orb^{F343} is a protein null, orb^{mel} is a weak hypomorph (Christerson and McKearin, 1994; Lantz et al., 1994). By western blot, we confirmed that Orb protein expression is reduced in *orb* mutant ovarian extracts (Fig. S2C,D),

Development (2022) 149, dev200426. doi:10.1242/dev.200426

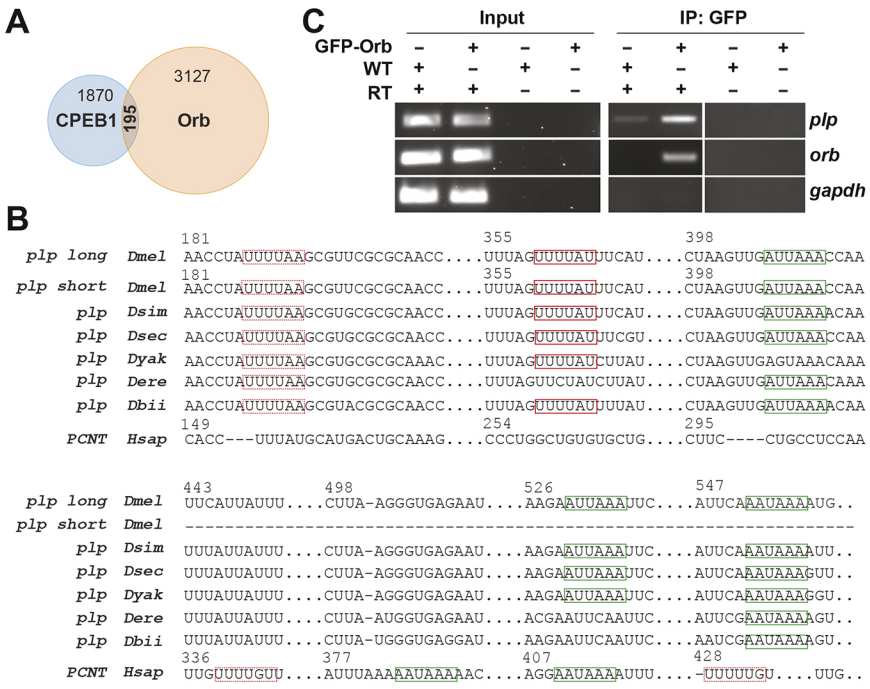

Fig. 2. *Plp* mRNA associates with Orb. (A) Venn diagram showing the common mRNA targets of CPEB1 and Orb (Stepien et al., 2016; Pascual et al., 2021). Table S2 lists overlapping mRNA targets. (B) Alignment of the *Plp* 3′UTRs from *Drosophila melanogaster* (*Dmel*), *D. simulans* (*Dsim*), *D. sechellia* (*Dsec*), *D. yakuba* (*Dyak*), *D. erecta* (*Dere*), *D. biarmipes* (*Dbii*) and human (*Hsap*) *PCNT* 3′UTRs (Goldman-Huertas et al., 2015; Larkin et al., 2021). Consensus (red solid boxes) and non-consensus (red dashed boxes) CPE motifs, and canonical CPSF A(A/U)UAAA hexamers (green boxes) are indicated. The nucleotide number of *D. mel Plp* and human *PCNT* 3′UTRs are listed above. (C) RNA immunoprecipitation from GFP-Trap beads using WT and *GFP-Orb* ovarian extracts. Input shows 10% of the total RNA. cDNAs were amplified with the indicated primers: *orb* is a positive control (Tan et al., 2001), *Gapdh1* is a negative control and *Plp* mRNA is 7.5-fold enriched in GFP-Orb relative to WT immunoprecipitated samples. Uncropped gels are available to view on Figshare: https://doi.org/10.6084/m9.figshare.16900417.v1.

consistent with prior work (Christerson and McKearin, 1994; Lantz et al., 1994). At all stages examined, we observed no difference in *Plp* or *Gapdh1* mRNA distributions in controls versus *orb* NC 10 or NC 12 mutant embryos (Fig. 3). These results indicate that Orb is not required for *Plp* mRNA localization to centrosomes.

Orb promotes PLP translation

Next, to investigate the contribution of Orb to regulation of PLP protein expression, we performed semi-quantitative western blotting to examine PLP levels in 0- to 2-h-old wild-type (WT) and *orb* mutant embryos. The *Plp* gene encodes 12 different protein isoforms varying in predicted molecular weight (MW) from ∼200 to 320 kDa (Graveley et al., 2011). Western blot analysis of 0- to 2-h-old embryonic extracts yielded multiple bands above 250 kDa. Comparing the banding pattern in control versus null Plp^{2172} mutant germline clones indicated that the band migrating just above 250 kDa is non-specific (asterisks), whereas the upper (caret; upper MW) and middle (arrowhead; mid-MW; Fig. S3A, Fig. 4) bands represent PLP isoforms migrating at different MWs. Consistent with this, multiple PLP isoforms have been detected in larval brains (Galletta et al., 2014). Because multiple PLP isoforms are predicted to migrate around the same MW, e.g. RF, RK, RL, RG, RP and RD

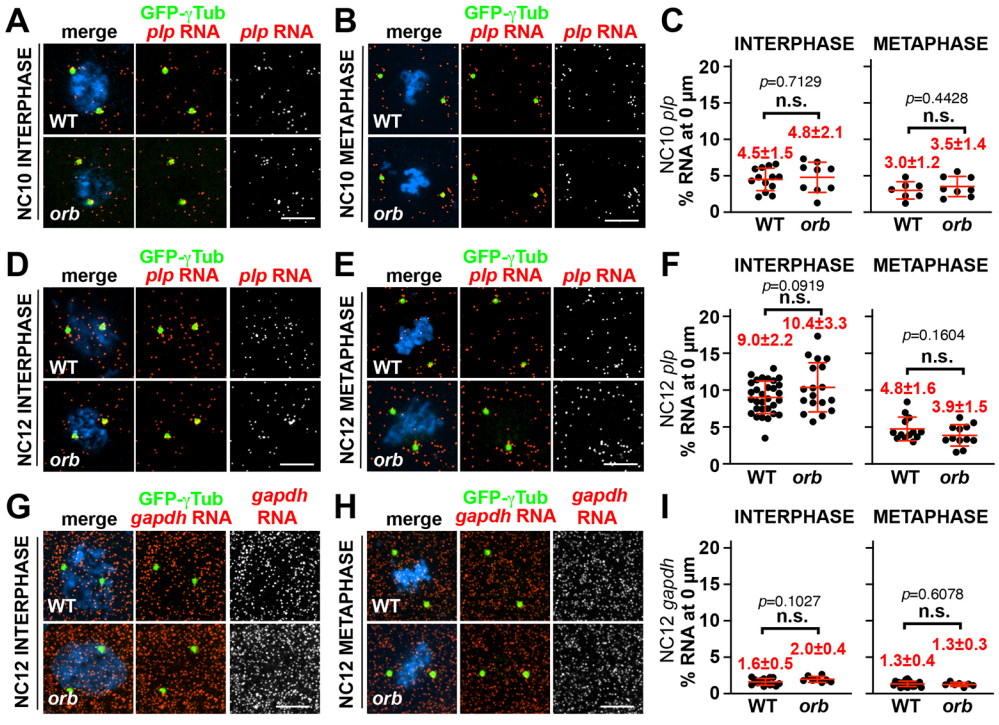

Fig. 3. Orb is dispensable for *Plp* mRNA localization. (A,B,D,E,G,H) Maximum intensity projections of NC 10 (A,B) or NC 12 (D,E,G,H) embryos of the indicated genotypes expressing *GFP-γTub* (green) and labeled with *Plp* or *Gapdh1* smFISH probes (red). (C,F,I) Quantification of *Plp* or *Gapdh1* mRNA localization to the centrosome surface in NC 10 or NC 12 embryos of the indicated genotypes. Table S1 lists the number of embryos, centrosomes and RNA objects quantified per condition. *orb* mutant: orb^{F343}/orb^{mel} mutant. Mean±s.d. are displayed. n.s., not significant by unpaired *t*-test. Scale bars: 5 µm.

Development (2022) 149, dev200426. doi:10.1242/dev.200426

migrate ∼320 KDa (caret; Fig. 4A-D), we are unable to distinguish individual isoforms. Instead, we quantified the upper versus mid-MW bands to calculate differences in PLP protein levels.

Quantification of the upper MW bands uncovered a ∼50% reduction in hypomorphic *orb* mutant embryos compared with WT (Fig. 4A,E). We recently showed that *Plp* hemizygous embryos (Plp^{2172}/+) also reduce PLP by about 40% (Fang and Lerit, 2020). Therefore, we generated Plp^{2172}, orb^{F343} recombinant chromosomes and crossed these animals to orb^{mel} mutants to harvest embryos from *Plp* hemizygous, *orb* mutant mothers (genotype: Plp^{2172}/+, orb^{F343}/orb^{mel}; hereafter, *Plp*/+, *orb*). Quantification shows that simultaneous depletion of *Plp* and *orb* within *Plp*/+, *orb* mutant embryos results in a ∼75% reduction of upper MW PLP products, suggesting that Orb regulates PLP translation (Fig. 4B,E). The mid-MW PLP isoforms may represent RM, RN and RJ and were similarly downregulated in *orb* embryos (Fig. 4A,F).

To investigate the specificity of the *orb*-dependent response on PLP expression, we also examined PLP levels after depleting the other *Drosophila* CPEB family member, Orb2, and Fragile X Mental Retardation Protein (FMRP; Fmr1), an RNA-binding protein known to share several common mRNA targets with *orb* (Costa et al., 2005). We note no significant difference in PLP levels in *orb2* or *Fmr1* null embryos (Fig. 4C-F). These results highlight a specific requirement of Orb to support normal levels of PLP protein, possibly at the level of translational activation.

Orb downregulates *Plp* mRNA levels

To investigate whether Orb regulates *Plp* mRNA levels to promote protein expression, we performed qRT-PCR using primers designed to recognize all predicted *Plp* mRNA variants. We detected a 1.3-fold increase in *Plp* mRNA in 0- to 2-h-old *orb*-depleted embryos relative to WT (Fig. S3B). Thus, the reduced levels of PLP protein observed in *orb* mutants may not be attributed to reduced *Plp* mRNA transcription or RNA stability.

During the first 2 h of embryogenesis, zygotic transcription is largely inhibited, and RNA is mainly acquired from maternal oocytes (Tadros and Lipshitz, 2009). To test whether the increased *Plp* mRNA observed in *orb* embryos might be inherited from oogenesis, we examined *Plp* mRNA in 2- to 4-day-old ovaries. *orb* ovarian extracts contained ∼1.4-fold more *Plp* mRNA than WT, suggesting that Orb normally attenuates *Plp* mRNA expression or stability and consistent with the idea that elevated levels of *Plp* mRNA in *orb* mutants are maintained in the early embryo (Fig. S3C). In contrast, we found that PLP protein levels are unaltered in *orb* mutant ovarian extracts compared with WT, indicating that Orb-dependent regulation of PLP translation is restricted to embryogenesis (Fig. S3D,E).

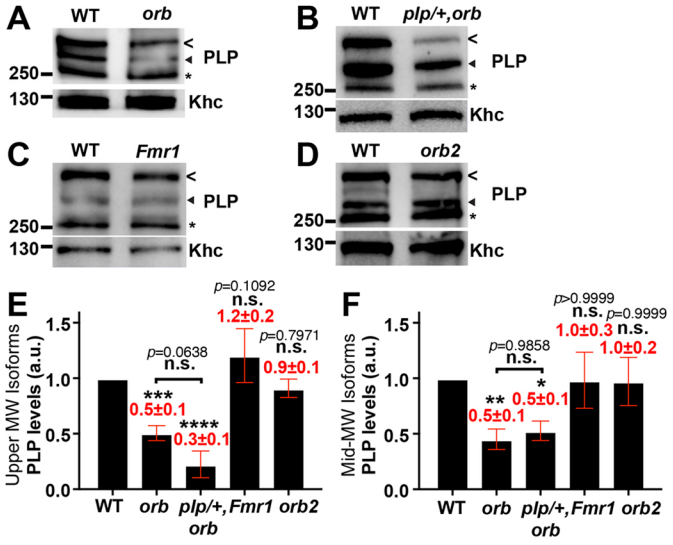

Fig. 4. Orb specifically promotes PLP protein expression.
(A-D) Immunoblots showing PLP levels relative to the Khc (anti-SUK4) load control in 0- to 2-h-old *Drosophila* embryo extracts from the indicated genotypes. *orb* mutant: orb^{F343}/orb^{mel}; *Plp*/+, *orb* mutant: Plp^{2172}/+, orb^{F343}/orb^{mel}. (E,F) Quantification of the relative levels of the upper MW PLP bands (carets) (E) and middle (mid-) MW PLP bands (arrowheads) (F) normalized to WT. Mean±s.d. are displayed. Significance was determined by one-way ANOVA with Dunnett's T3 multiple comparisons test relative to WT unless otherwise noted. n.s., not significant; *P<0.05; **P<0.01; ***P<0.001; ****P<0.0001. Uncropped blots are available to view on Figshare: https://doi.org/10.6084/m9.figshare.16900423.v1.

Orb facilitates the polyadenylation of *Plp* mRNA

CPEB proteins, including Orb, mediate translational activation and/or repression by regulating the cytoplasmic polyadenylation of target mRNAs (Chang et al., 1999, 2001; Castagnetti and Ephrussi, 2003; Kim and Richter, 2007; Novoa et al., 2010; Burns et al., 2011; Norvell et al., 2015; Rojas-Ríos et al., 2015). To examine whether Orb regulates *Plp* mRNA polyadenylation to promote PLP translation, we monitored *Plp* poly(A) tail length. Among the 12 *Plp* mRNA variants, only Plp^{RM} uses the long 3′UTR (591 nt). The remaining 11 *Plp* mRNA variants use a short 3′UTR (431 nt) (Fig. 5A) (Graveley et al., 2011). We first assayed which *Plp* 3′ UTRs are expressed in 0- to 2-h-old embryos by amplifying cDNA using one of two reverse primers: one aligns within a region common to both *Plp* 3′UTRs (Plp_{Rev1}), whereas the other specifically aligns to the long *Plp* 3′UTR (Plp_{Rev2}; Fig. 5A). PCR products corresponding to the *Plp* 3′UTR were further validated by restriction enzyme digestion (Norvell et al., 2015). Whereas both *Plp* 3′UTRs are sensitive to BmrI digestion, only the long *Plp* 3′ UTR is sensitive to EcoR1 (Fig. 5A,B, lanes 1-8). Although our PCR profiling confirmed expression of the long 3′UTR associated with Plp^{RM}, qRT-PCR demonstrated that Plp^{RM} represents only ∼5% of total *Plp* mRNA in 0- to 2-h-old WT embryos (Fig. 5C). Bioinformatic analysis of published RNA-sequencing datasets confirms the lower expression of Plp^{RM} in early embryos (Graveley et al., 2011).

We next performed a poly(A) test (PAT) assay of *Plp* mRNA from control versus orb^{F343}/orb^{mel} mutant embryos (Legnini et al., 2019). For this, we tagged polyadenylated mRNA from 0- to 2-h-old embryos with guanosine and inosine (G/I-tailing), followed by RT-PCR to synthesize cDNA. *Plp* poly(A) tails were then amplified by PCR using a universal reverse primer and a *Plp*-specific forward primer (Fig. 5A). PAT products resolved as a ∼339-525 bp smear by gel electrophoresis (Fig. 5B, lanes 9, 10), corresponding to approximately 14-200 nt poly(A) length (Fig. 5B, arrowheads). Based on the position of our Plp_{Rev1} primer, products below 293 bp [i.e. below 0 nt poly(A) length for the short 3′UTR] likely represent non-specific bands; these were detected in all PAT samples (Fig. 5B, lanes 9-14). We used restriction enzyme digestion to distinguish PAT products from the *Plp* long versus short 3′-UTRs. As *Plp* PAT products are sensitive to BmrI digestion, but only modestly altered by EcoRI, we conclude that polyadenylated products from the short *Plp* 3′UTR are more enriched in 0- to 2-h-old embryos than those from the long *Plp* 3′-UTR (Fig. 5B, lane 9-14). Plotting a line profile of the PAT products detected in control versus *orb* embryos reveals a leftward shift indicative of reduced polyadenylation of *Plp* mRNA in *orb* mutants (Fig. 5D,

Development (2022) 149, dev200426. doi:10.1242/dev.200426

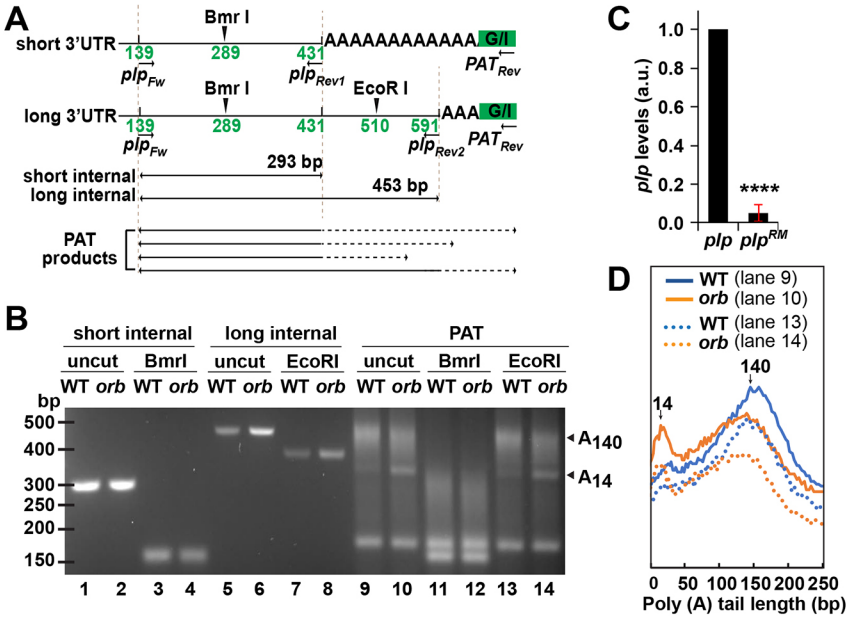

Fig. 5. Orb promotes *Plp* polyadenylation. (A) Diagram showing the PCR primers and EcoRI and BmrI restriction sites on the short and long *Plp* 3′UTRs. The predicted sizes of internal PCR products are listed below. (B) cDNA products amplified from G/I-tailed RNA extracted from 0- to 2-h-old control (*iso-1*) and orb^{F343}/orb^{mel} embryos. PCR products were digested with EcoRI or BmrI, as indicated. The approximate lengths of poly(A)-tails are noted (arrowheads). (C) Relative levels of total *Plp* mRNA and Plp^{RM} mRNA normalized to *RP49* mRNA were examined by qRT-PCR in 0- to 2-h-old WT embryos; ****P<0.0001 by unpaired *t*-test. a.u., arbitrary units. (D) Line profiles from undigested (solid lines; lanes 9, 10) and EcoR1-digested (dashed lines; lanes 13, 14) PAT products. Poly(A)-tail length was calculated by subtracting the internal PCR product plus G/I tail length from the total PAT product length. Uncropped gel is available to view on Figshare: https://doi.org/10.6084/m9.figshare.16900471.v4.

solid lines). Similar results were observed in replicated experiments (Fig. S3F,G). To confirm that the short *Plp* 3′UTR is differentially polyadenylated in controls versus *orb* mutants, we also examined the profiles of the EcoRI-digested PAT products, which should be enriched for the polyadenylated short *Plp* 3′UTR. This analysis also revealed a leftward shift (Fig. 5D, dashed lines). Because polyadenylation stimulates translation (Eichhorn et al., 2016; Passmore and Coller, 2021; Xiang and Bartel, 2021), our results are consistent with a model wherein Orb activates *Plp* mRNA translation by promoting polyadenylation of the short 3′UTR.

Orb regulates PLP-Cnn scaffold organization

In interphase embryos, PLP normally localizes to the centriole and at the tips of extended PCM flares (Lerit et al., 2015; Richens et al., 2015). To investigate whether the depletion of PLP protein observed in *orb* mutants alters PLP localization to the centrosome, we quantified the intensity of endogenous PLP signals at control versus *orb* mutant centrosomes in NC 13 embryos. As expected, WT embryos had PLP signals at the centriole and flare zone (Fig. 6A, WT). We generated *Plp* null mutant germline clone embryos (*Plp* mutants) and confirmed that PLP is undetectable, validating the specificity of our antibody (Fig. 6A, *Plp*). In contrast, *orb* mutants, *Plp*/+ hemizygotes and recombinant *Plp*/+, *orb* mutant embryos showed reduced PLP localization to centrosomes compared with WT (Fig. 6A; *orb*, *Plp*/+ and *Plp*/+, *orb*). To quantify the relative localization of PLP at centrosomes, we used a custom Python code to batch calculate the total intensity of PLP signals within 2 µm of the centrosome across all genotypes after validating this approach by comparison with manual quantification (Fig. S4A-C). Quantification uncovered a ∼20% reduction of PLP at centrosomes in *orb* mutants and *Plp*/+ hemizygotes, which, although not significantly different from WT by one-way ANOVA, trends downward (Fig. 6B). Given that orb^{mel} is a hypomorph, not a null allele, and some functional Orb protein remains in orb^{F343}/orb^{mel} mutants (Fig. S2C), PLP recruitment to centrosomes is likely to be further reduced in the absence of *orb* activity. Consistent with a requirement for *orb* in PLP localization, we noted a ∼20% reduction in recombinant *Plp*/+, *orb* mutants compared with *Plp*/+, which also trends lower but was not significantly different by one-way ANOVA (Fig. 6A,B). These data suggest that PLP dosage at centrosomes is sensitive to *orb* activity.

We reasoned that the apparent reduction in PLP recruitment to centrosomes might be attributed to the reduction in total PLP levels, suggesting that increasing *Plp* dosage should rescue PLP localization in *orb* embryos. To test this hypothesis, we expressed in the *orb* mutant background a functional *PLP-GFP* transgene capable of rescuing *Plp* mutant phenotypes (Galletta et al., 2014; Lerit et al., 2015). PLP distribution is restored at *PLP-GFP; orb* centrosomes, supporting the idea that PLP localization to centrosomes occurs downstream of *orb* activity (Fig. 6A, B; P<0.05 for *PLP-GFP; orb* versus *orb* and P=0.4978 for *PLP-GFP; orb* versus WT by one-way ANOVA).

Our prior work showed that PLP interacts directly with and organizes Cnn at centrosomes to support PCM scaffolding (Lerit et al., 2015). Given the diminished PLP levels detected in *orb* mutants, we next assayed Cnn organization. In control embryos, Cnn radiated symmetrically from centrosomes, forming interphase-specific flares, as previously described (Fig. 6C, WT) (Megraw et al., 2002). Consistent with our prior work, Cnn distribution appeared severely disorganized in *Plp* embryos with Cnn fragments dispersed within the cytosol (Fig. 6C, *Plp*) (Lerit et al., 2015; Fang and Lerit, 2020). Quantification of the relative number of cytoplasmic Cnn puncta in segmented images showed a significant, nearly 6-fold increase in *Plp* embryos relative to WT (Fig. 6D; P<0.001 by one-way ANOVA). Similar responses, albeit with reduced magnitude, were also observed in *orb* and *Plp*/+, *orb* mutant embryos (Fig. 6C,D; P<0.01 for *orb* and P<0.001 for *Plp*/+, *orb* versus WT by one-way ANOVA). In contrast, the relative number of cytoplasmic Cnn puncta in *Plp*/+ hemizygotes trended upward but was not significantly different from WT (Fig. 6C,D; *Plp*/+). Moreover, expression of the *PLP-GFP* transgene rescued Cnn organization in *orb* mutants (Fig. 6C,D; P=0.9662 for *PLP-GFP; orb* versus WT by one-way ANOVA). Therefore, Orb contributes to proper PLP-Cnn scaffold organization, likely by regulating PLP protein expression and localization.

Orb protein distributes throughout the somatic cytoplasm

As Orb associates with *Plp* mRNA and potentiates PCM scaffolding, we next ascertained whether endogenous Orb protein localizes near centrosomes. In syncytial blastoderm embryos, Orb signals are enriched within the pole cells at the posterior pole (Lantz

Development (2022) 149, dev200426. doi:10.1242/dev.200426

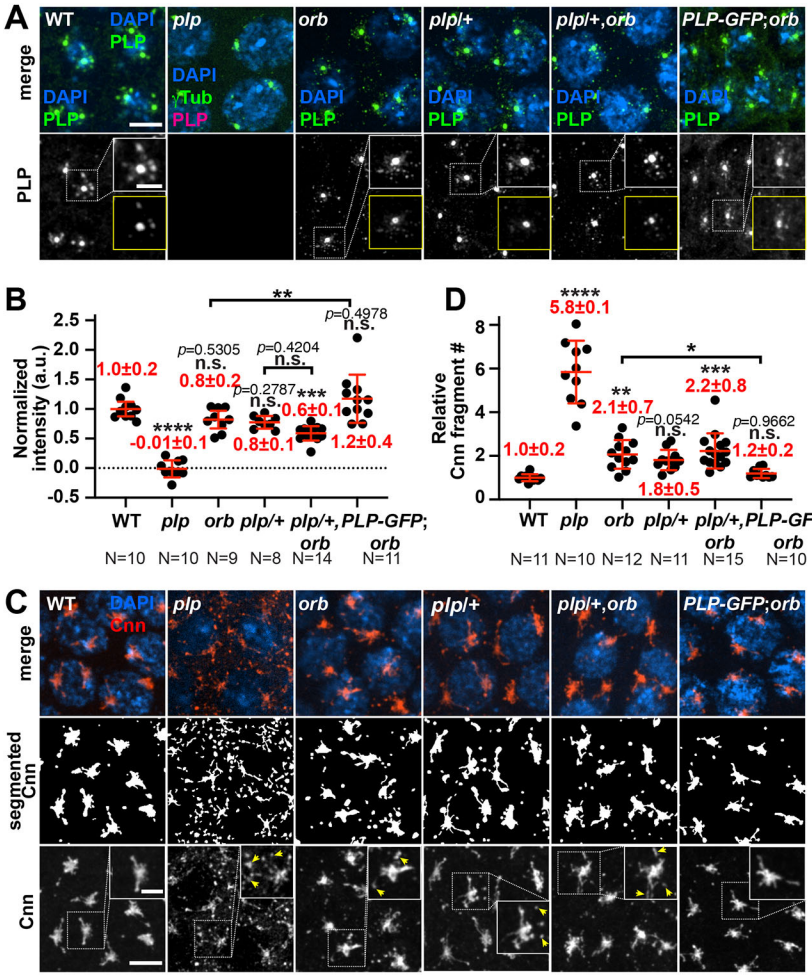

Fig. 6. Formation of the PLP-Cnn PCM scaffold requires Orb. (A) Maximum intensity projections of NC 13 embryos of the indicated genotypes stained with anti-PLP antibodies. The same LUT was used to display PLP signals in all genotypes to highlight PLP within the flare-zone. Boxed regions are enlarged in the insets, and less-saturated images are shown in the yellow boxes. (B) Quantification of PLP intensity within 2 µm of the centrosome. Values were normalized to the mean intensity from WT embryos. Each circle represents the PLP intensity of one embryo averaged from all centrosomes in a 65 µm^2 region. (C) Top and bottom: Maximum intensity projections of NC 13 embryos stained with anti-Cnn antibodies (red). Yellow arrowheads highlight Cnn fragments. Boxed regions are enlarged in the insets. Middle: Segmented Cnn images. (D) Quantification of the number of Cnn fragments normalized to the WT mean. Each circle represents the relative number of Cnn fragments of one embryo averaged from all centrosomes in a 65 µm^2 region. Significance was determined by one-way ANOVA followed by Dunnett's T3 multiple comparisons test relative to WT. n.s., not significant; *P<0.05; **P<0.01; ***P<0.001; ****P<0.0001. Genotypes used were: *orb* mutant: orb^{F343}/orb^{mel}; *Plp*/+ hemizygote: Plp^{2172}/+; *Plp*/+, *orb* mutant: Plp^{2172}/+, orb^{F343}/orb^{mel}; *PLP-GFP; orb* mutant: *PLP-GFP;* orb^{F343}/orb^{mel}. Mean±s.d. are displayed. Scale bars: 5 µm (main panels); 2 µm (insets).

et al., 1992; Rangan et al., 2009). In addition, we observed some Orb apposed centrosomes within somatic, mid-embryo regions (Fig. S4D, control). As expected, anti-Orb signals were diminished in hypomorphic *orb* mutants (Fig. S4D, $orb^{F343/mel}$). These data suggest that Orb may regulate mRNA targets locally at the centrosome, within the cytoplasm, or both.

Orb-dependent regulation of PLP supports genome stability

A requirement for Orb in modulating PLP levels, localization and activity predicts that loss of *orb* would compromise centrosome function in maintaining mitotic fidelity. To investigate whether *orb* depletion is associated with chromosome instability (CIN), we stained WT and *orb* mutant embryos with DAPI, the mitotic marker pH3 and Asterless (Asl) to label centrioles (Varmark et al., 2007). Upon examination of anaphase embryos, the chromosomes in WT samples completely separated and lagging chromosomes were infrequent (n=3/20 WT embryos with CIN; Fig. 7A,B). In contrast, elevated rates of lagging chromosomes or chromosomal bridges were observed in *orb* mutants (55%, n=11/20 *orb* embryos with CIN), represented by lagging chromosomes at the spindle equator with persistent pH3-staining in anaphase/telophase-stage embryos (Fox et al., 2010; Vitre and Cleveland, 2012). Moreover, *PLP-GFP* expression restored the mitotic fidelity of *orb* mutant embryos, evident by decreased CIN rates (21%, n=5/24 *PLP-GFP; orb* embryos with CIN; Fig. 7A,B; P<0.01 for *PLP-GFP; orb* versus *orb* and P=0.4995 for *PLP-GFP; orb* versus WT by χ^2 analysis).

To examine further the extent of CIN within individual embryos, we quantified the proportion of nuclei exhibiting CIN from genotype-blinded images. These data confirmed that the frequency of CIN is elevated in *orb* mutants. Although n=3/20 WT embryos displayed CIN, only one embryo had ∼20% nuclei with CIN; the other two embryos had ∼1% nuclei with CIN. In contrast, most *orb* mutant embryos had significantly more (5-47%) CIN^+ nuclei (P<0.01 for WT versus *orb* by one-way ANOVA followed by Kruskal–Wallis test; Fig. 7C). *PLP-GFP* expression significantly alleviated the CIN defects in *orb* mutants (5-20%; P<0.05 for *PLP-GFP; orb* versus *orb* and P>0.9999 for *PLP-GFP; orb* versus WT by one-way ANOVA followed by Kruskal–Wallis test; Fig. 7C). Taken together, these data indicate a requirement for *orb* in preserving genome stability by a mechanism dependent upon PLP dosage.

To examine genome stability further, we measured rates of nuclear fallout (NUF), a developmental response to DNA damage in which damaged nuclei are ejected from the syncytial blastoderm cortex and targeted for apoptosis (Sullivan et al., 1993; Rothwell et al., 1998). NUF is readily detected as gaps in the normally uniform monolayer of DAPI-positive nuclei lining the embryonic cortex (Fig. 7D, dashed lines). Although low rates of NUF were apparent even in WT embryos (7%, n=2/30), we observed significantly more NUF in *orb* mutants (47%, n=17/36; Fig. 7D, E; P<0.001 by χ^2 analysis). However, NUF was rescued in *orb* mutants expressing the *PLP-GFP* transgene (16%, n=6/36 *PLP-GFP; orb* embryos with NUF; Fig. 7D,E; P<0.01 for *PLP-GFP;*

Development (2022) 149, dev200426. doi:10.1242/dev.200426

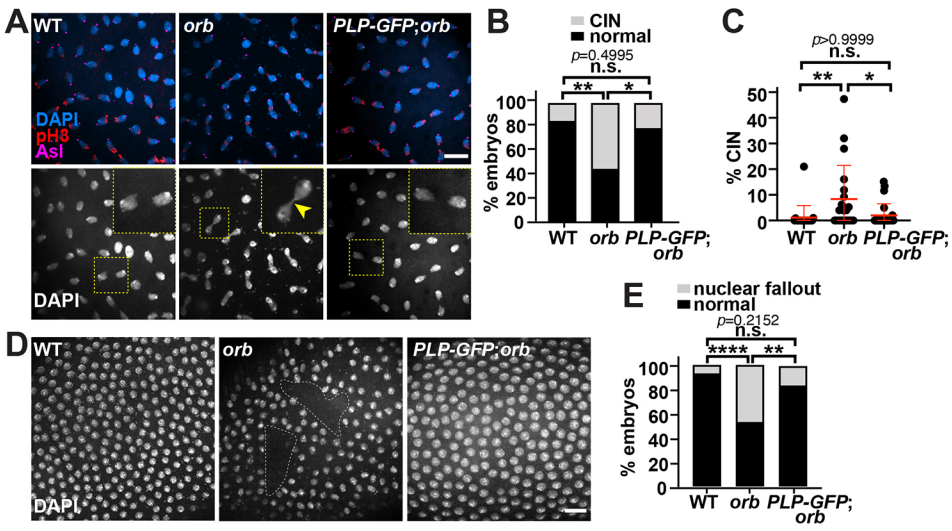

Fig. 7. Orb functions upstream of PLP to support mitotic fidelity. (A) Maximum intensity projections of NC 12 telophase embryos labeled with anti-pH3 (red) and Asl (magenta) antibodies to visualize chromosome separation. Boxed regions are enlarged in the insets. Yellow arrowhead indicates an anaphase bridge. (B) Percentage of embryos with CIN. (C) Quantification of the proportion of CIN per embryo. Error bars show mean±s.d. (D,E) Maximum intensity projections of NC 13 interphase embryos labeled with DAPI to reveal NUF (D), with quantification in E. Significance was determined by χ^2 analysis (B,E) or one-way ANOVA followed by Kruskal–Wallis multiple comparisons test (C). n.s., not significant; *P<0.05; **P<0.01; ****P<0.0001. *orb* mutant: orb^{F343}/orb^{mel}; *PLP-GFP; orb* mutant: *PLP-GFP;* orb^{F343}/orb^{mel}. Scale bars: 20 µm.

orb versus *orb* and P=0.2152 for *PLP-GFP; orb* versus WT by χ^2 analysis), further supporting the idea that Orb promotes genome stability via PLP.

To examine the mitotic fidelity of *orb* mutants in greater detail, we examined mitotic progression in live, cycling embryos expressing *GFP-γTub* to label the centrosomes and *H2A-RFP* to follow the chromosomes. As we were unable to recover double-balanced orb^{F343} mutants, for these experiments we employed the weaker transheterozygous combination orb^{F303}/orb^{mel} to deplete Orb (Lantz et al., 1994) (Fig. S2D). Whereas nuclei synchronously divided without NUF in most control embryos (18%, n=2/11 showed NUF; Fig. 8A, Movie 1), about 50% of orb^{F303}/orb^{mel} embryos displayed NUF (N=5/10 showed NUF; Fig. 8B, Movie 2). Consistent with our quantification using fixed samples, expression of the *PLP-GFP* transgene largely ameliorated NUF in *orb* mutant embryos (17%, n=1/6 showed NUF; Fig. 8C, Movie 3), supporting a model wherein Orb contributes to centrosome function by regulating PLP.

Disruption of centrosome function impairs genome stability, which typically manifests as elevated rates of embryonic lethality. We conducted hatch-rate analysis to approximate embryonic viability in *orb* mutants versus controls. Relatively low rates of embryonic lethality were noted in WT embryos, as nearly 90% hatched to first-instar larvae. In contrast to WT and consistent with previous studies (Christerson and McKearin, 1994; Lantz et al., 1994), only 32% of orb^{F343}/orb^{mel} mutants hatched to first-instar larvae (Table 1). Embryonic lethality in *orb* mutants is largely attributed to the requirement of Orb in establishing the embryonic patterning axes via its role in mediating localization and translation of *osk* and *grk* mRNAs (Christerson and McKearin, 1994; Chang et al., 1999, 2001; Castagnetti and Ephrussi, 2003). Interestingly, expression of the *PLP-GFP* transgene partially restored embryonic viability (53% hatched; P<0.0001, *orb* versus *PLP-GFP*; *orb* by χ^2 test) (Table 1), supporting the suggestion that a genetic interaction between *orb* and *Plp* is required for viability. Orb further supports embryonic viability by regulating other mRNA targets or protein

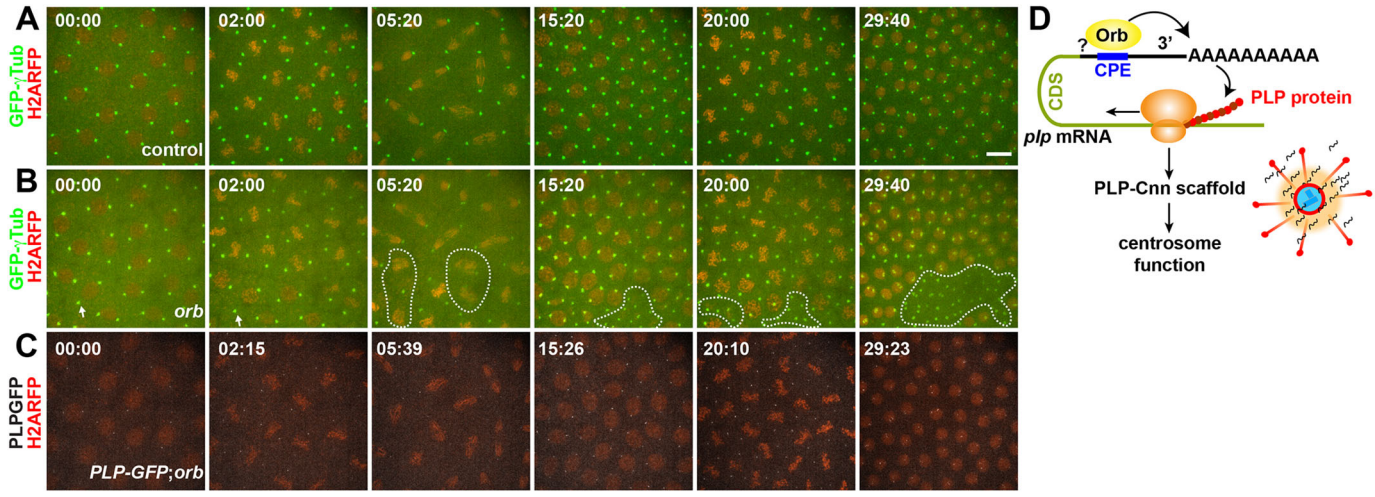

Fig. 8. Orb promotes genome stability via PLP. Maximum intensity projected stills from time-lapse imaging of *GFP-γTub* or *PLP-GFP* with *H2A-RFP* in control (A), orb^{F303}/orb^{mel} mutant (B) and *PLP-GFP;* orb^{F303}/orb^{mel} (C) embryos. Time is in min:s. Dashed lines mark NUF. Stills correspond to Movies 1-3. (D) Proposed model for Orb-mediated regulation of *Plp* mRNA by promotion of *Plp* polyadenylation. Orb associates with *Plp* mRNA; this interaction may be direct through CPE motifs in the 3′UTR or indirect. Orb promotes the polyadenylation of *Plp* mRNA, which contributes to PLP protein synthesis. PLP expression supports the PLP-Cnn scaffold assembly necessary for centrosome function and error-free mitosis. Scale bar: 10 µm.

Development (2022) 149, dev200426. doi:10.1242/dev.200426

Table 1. Quantification of embryonic hatch rates from the indicated genotypes

Genotype	Total	Unhatched	Hatched	Hatch rate	Significance*
WT	712	86	626	88%	N/A
orb	749	513	236	32%	$P<0.0001$ compared with WT
PLP-GFP; orb	622	329	293	47%	$P<0.0001$ compared with WT $P<0.0001$ compared with *orb*

*Fisher's exact test

partners (Chang et al., 2001; Mansfield et al., 2002; Norvell et al., 2015). Nonetheless, our data argue *Plp* is likely a downstream target subject to Orb regulation and support a model in which Orb activates *Plp* mRNA translation by promoting polyadenylation. This regulation is crucial for PLP-Cnn scaffold assembly, which is required for centrosome function and viability (Table 1). Our findings highlight that the translational regulation of centrosomal mRNAs is important for centrosome activity and function and indicate that Orb is important for centrosome function.

DISCUSSION

We recently analyzed the distributions of five centrosomal mRNAs, including *Plp* mRNA, revealing a common cell cycle-dependent enrichment at late interphase centrosomes (Ryder et al., 2020). Our present work extended this analysis, highlighting enrichment of *Plp* mRNA at centrosomes across syncytial development. One simple model is that centrosomal mRNAs are more likely to localize to interphase centrosomes, which are larger than mitotic centrosomes in syncytial *Drosophila* embryos (Megraw et al., 2002; Lerit et al., 2015). This model oversimplifies the specificity of RNA localization to centrosomes – relatively few RNAs reside at centrosomes (Lécuyer et al., 2007; Chouaib et al., 2020; Kwon et al., 2021; Safieddine et al., 2021). Moreover, similar interphase/prophase-stage preferential enrichments of centrosomal mRNAs were recently observed in cultured human cells, wherein centrosome size is larger in mitosis (Sepulveda et al., 2018; Safieddine et al., 2021). Collectively, these studies demonstrate that multiple mRNAs across divergent species co-enrich at centrosomes at the same cell cycle phase, suggestive of conserved localization mechanisms (Zein-Sabatto and Lerit, 2021). How RNA localization to centrosomes is executed at the molecular level in a cell cycle-dependent manner is a fascinating question requiring further investigation.

Toward this end, we identified conservation of multiple CPE sites within the *Plp* and *PCNT* 3′UTRs. Because CPE-containing mRNAs are enriched at spindle poles and CPEB is required for *cyclin B1* mRNA localization (Groisman et al., 2000), we reasoned that CPE sites may contribute to *Plp*, and possibly *PCNT*, mRNA localization. Given its established roles in mediating localization of other mRNAs, such as *osk* and *grk*, we hypothesized that Orb might contribute to the enrichment of *Plp* mRNA to centrosomes. Our data do not support this hypothesis. Strong hypomorphic *orb* mutant embryos did not exhibit disrupted *Plp* mRNA localization to centrosomes.

In cell culture models, *PCNT* mRNA localization to the centrosome is puromycin sensitive, suggesting that it is trafficked by a co-translational transport mechanism (Sepulveda et al., 2018; Safieddine et al., 2021). Although *orb* depletion does not impair *Plp* mRNA localization to centrosomes, it does reduce multiple PLP isoforms by about 50%, suggesting that RNA localization and translation may be uncoupled. It is feasible that multiple *orb*-independent mechanisms contribute to *Plp* mRNA localization to centrosomes. Furthermore, our data show that multiple PLP isoforms are subject to Orb regulation. Whether the various PLP isoforms have different functions or regulatory mechanisms is an interesting topic for future study.

Our data support a model whereby Orb regulates PLP translational activation by facilitating polyadenylation. We identified a conserved hexanucleotide motif (AAUAAA) that is important for translational control just downstream of a CPE motif in the *Plp* 3′UTR. This proximity is predicted to modulate the extent of polyadenylation and translational activation (Piqué et al., 2008). In many organisms, the first hours of embryogenesis rely upon maternally provided mRNAs and proteins until the maternal-to-zygotic transition activates bulk zygotic transcription (Tadros and Lipshitz, 2009). Consequently, translational regulation is a signature paradigm of gene regulation during early development (Johnstone and Lasko, 2001). Because syncytial *Drosophila* embryos divide every 10-20 min, they undergo rapid, successive centrosome doubling events and oscillations in PCM recruitment and shedding at compressed timescales. Here, we define a mechanism of translational activation of a conserved PCM scaffolding factor, PLP, mediated by the CPEB family member Orb. Future work is needed to determine whether Orb binds *Plp* mRNA directly to stimulate local translation of *Plp* mRNA at centrosomes.

We detected differential usage among two alternative 3′UTRs, showing that the shorter *Plp* 3′UTR is favored during embryogenesis. Moreover, monitoring poly(A)-tail length revealed reduced polyadenylation at the shorter *Plp* 3′UTR in *orb* mutants compared with controls. Genome-wide studies have revealed that mRNA poly(A) length is generally positively correlated with translation efficiency in *Drosophila* mature oocytes and early embryos (Subtelny et al., 2014; Eichhorn et al., 2016; Lim et al., 2016). Other studies using luciferase reporter systems have also demonstrated that poly(A)-tail length strongly influences translation efficiency (Coll et al., 2010; Xiang and Bartel, 2021). Consistent with this model, the poly(A)-tail length of the Orb target mRNAs, *cortex* (*cort*), *osk* and *Atg12* correlate with translational efficiency (Castagnetti and Ephrussi, 2003; Benoit et al., 2008; Rojas-Ríos et al., 2015). Thus, polyadenylation by Orb likely promotes *Plp* mRNA translation.

The mechanism by which CPEB proteins promote translation is best defined in *Xenopus* oocytes and embryos; in immature oocytes or during embryonic progression into M phase, CPE-containing mRNAs are translationally repressed in a complex with CPEB and Maskin, an EIF4E-binding protein that inhibits polyadenylation-dependent translation activation (Mendez et al., 2000b; Groisman et al., 2002). When oocyte maturation begins or embryos exit M phase, this inhibition is relieved by CPEB1 phosphorylation, which triggers dissociation of Maskin from EIF4E and recruits CPSF and poly(A) polymerase (PAP) to the 3′UTR of mRNA targets to elongate their poly(A)-tails. The polyadenylated mRNA then recruits and stabilizes interactions with poly(A)-binding protein (PABP) and further recruits eukaryotic translation initiation factors, leading to ribosome assembly and protein translation (Groisman et al., 2000; Mendez et al., 2000b; Mendez and Richter, 2001;

Development (2022) 149, dev200426. doi:10.1242/dev.200426

Groisman et al., 2002). The requirement of PAP for Orb-dependent polyadenylation of *cort* mRNA in *Drosophila* oocytes indicates that mechanisms of CPEB translational regulation are likely conserved (Benoit et al., 2008).

Although PLP protein levels are diminished in *orb* mutants, PLP localization to centrosomes is more modestly impaired. We detected ∼20% less PLP localizing to interphase centrosomes in NC 13 *orb* embryos versus ∼50% less PLP protein in embryonic extracts pooled across NC 1 to NC 14. This variance may be attributed to cell cycle or NC-specific dynamics of PLP protein expression or localization. In addition, perdurance of PLP protein at the centrosome may be due to its relatively slow rate of turnover (Conduit et al., 2014; Richens et al., 2015). Moreover, because null *orb* mutants do not produce embryos (Lantz et al., 1994), we characterized embryonic *orb* phenotypes in a hypomorphic orb^{F343}/orb^{mel} background, wherein small amounts of functional Orb protein remain. Thus, changes to PLP expression, localization to centrosomes, and associated phenotypes would likely be exacerbated in the complete absence of *orb* activity. Furthermore, Orb may regulate other mRNAs, such as *spd*-2 or *polo*, to enhance PCM recruitment and support centrosome activity. Taken together, our data are consistent with a model whereby Orb-mediated translational activation of *Plp* mRNA facilitates PLP protein localization to centrosomes (Fig. 8E), although redundant mechanisms likely exist to ensure robust localization, consistent with the integral role PLP plays in PCM scaffolding.

MATERIALS AND METHODS

Fly stocks

The following stocks and transgenic lines were used: y^1w^{1118} [Bloomington *Drosophila* Stock Center (BDSC) #1495] was used as the WT control unless otherwise noted. The genome reference genotype *iso-1* (BDSC #2057) was used as the control for the PAT assay (Brizuela et al., 1994). In all experiments except for live imaging, *orb* mutant embryos were orb^{F343}/orb^{mel} transheterozygotes [orb^{F343}, BDSC #58477 (Lantz et al., 1994) and orb^{mel}, BDSC #58743 (Christerson and McKearin, 1994)]. For live imaging, orb^{F303}/orb^{mel} transheterozygotes were used (Christerson and McKearin, 1994; Lantz et al., 1994). Null *Fmr1* mutant embryos were $Fmr1^{\Delta 113M}/Fmr1^3$ transheterozygotes [$Fmr1^{\Delta 113M}$, BDSC #67403; $Fmr1^3$, a gift from T. Jongens, University of Pennsylvania, USA (Dockendorff et al., 2002)]. Null *orb2* mutant embryos were $orb2^{36}/orb2^7$ transheterozygotes ($orb2^7$, BDSC #58480; $orb2^{36}$, BDSC #58479; Xu et al., 2012); Plp^{2172} allele is a null allele (Spradling et al., 1999; Martinez-Campos et al., 2004) and was recombined onto the orb^{F343} chromosome to generate Plp^{2172}, orb^{F343} recombinant animals. Null *Plp* mutant germline clones were generated by the FLP/ovoD method using *FRT2A*, Plp^{2172} recombinant chromosomes (Chou and Perrimon, 1996; Lerit et al., 2015). *Ubi-GFP-γ-Tub23C* expresses GFP-γTub under the *Ubiquitin* (*Ubi*) promotor (Lerit and Rusan, 2013); $Ubi\text{-}PLP^{FL}\text{-}GFP$ expresses the full-length PLP isoform PF under the *Ubi* promoter (Galletta et al., 2014); *H2A-RFP* expresses a red fluorescent H2A variant under endogenous regulatory elements (Pandey et al., 2005); and *GFP-Orb* is a gene trap expressing a GFSTF (EGFP, FlAsH, StrepII, TEV and 3xFLAG) tag under endogenous regulatory elements (BDSC #59817; Nagarkar-Jaiswal et al., 2015). To examine maternal effects, mutant embryos were progeny derived from mutant mothers. Flies were raised on Bloomington formula 'Fly Food B' (LabExpress), and crosses were maintained at 25°C in a light- and temperature-controlled incubator chamber.

Bioinformatics

To compare overlapping mRNA targets of Orb (Stepien et al., 2016) and CPEB1 (Pascual et al., 2021), *Drosophila* gene names were converted to human gene identifiers using the of Query symbols/IDs tool in FlyBase (Larkin et al., 2021). Overlapping genes were identified by the 'COUNT IF' function in Excel. Venn diagrams were plotted using the Meta-Chart online tool (https://www.meta-chart.com/). Gene ontology cellular component analysis of common genes was analyzed using the Panther statistical over-representation test (http://www.pantherdb.org/), and Fisher's exact test was used to generate an adjusted *P*-value, i.e. false discovery rate (FDR) (Mi et al., 2021).

To align human *PCNT* (NCBI; NM_006031.6) and *Drosophila Plp* 3′ UTRs, Clustal Omega was used (Madeira et al., 2019). Conservation of CPE motifs with the *Plp* 3′UTRs from different *Drosophila* species was compared using the conservation 124 insect track on the UCSC genome browser (Kent et al., 2002).

Embryonic hatch rate analysis

Eggs (6-12 h) were collected on yeasted grape juice agar plates and ∼200 embryos were transferred to fresh plates and aged for 48 h at 25°C. Unhatched embryos were counted from each plate as a proxy for embryonic lethality, and three independent replicates were performed. Although not directly quantified, we did not observe elevated rates of unfertilized embryos in our *orb* mutant samples during centrosome structure or mitotic fidelity analyses.

Live imaging

Embryos were prepared for live imaging as described by Lerit et al. (2017). Briefly, dechorionated embryos were adhered to a sticky 22×30 mm #1.5 glass coverslip, covered with a thin layer of halocarbon oil, and inverted onto a clear, gas-permeable 50 mm dish using broken #1 glass coverslips as spacers. Images were captured at 1 µm *z*-intervals over a 10-15 µm volume at 20 s intervals.

Immunofluorescence

For immunofluorescence with PLP and Cnn antibodies, embryos were fixed in a 1:1 solution of anhydrous methanol (Sigma-Aldrich, 322415):heptane for 15 s and devitellinized in methanol. For smFISH and immunofluorescence staining with Asl and pH3 antibodies, embryos were fixed in a 1:4 solution of 4% paraformaldehyde:heptane for 20 min and devitellinized in methanol (Rothwell and Sullivan, 2007). Fixed embryos were rehydrated, blocked in BBT buffer [PBS supplemented with 0.1% Tween-20 and 0.1% bovine serum albumin (BSA)], and incubated overnight at 4°C with primary antibodies diluted in BBT. For Asl staining, BBT buffer with 0.5% BSA was used. After washing, embryos were further blocked in BBT supplemented with 2% normal goat serum and incubated for 2 h at room temperature with secondary antibodies and DAPI (10 ng/ml, Thermo Fisher Scientific). Embryos were mounted in Aqua-Poly/Mount (Polysciences) prior to imaging.

The following primary antibodies were used: rabbit anti-PLP antibody (1:4000, gift from N. Rusan, National Institutes of Health), guinea pig anti-Asl (1:4000, gift from G. Rogers, University of Arizona, USA), rabbit anti-Cnn (1:4000, gift from T. Megraw, Florida State University, USA), mouse anti-phospho-Histone H3 Ser10 (pH3; 1:1000, Millipore 05570) and mouse anti-Orb [1:10; Developmental Studies Hybridoma Bank (DSHB) 6H4; P. Schedl, Princeton University, USA). Alexa Fluor 488-, 568- or 647-secondary antibodies were used (1:500, Molecular Probes) (see Table S3).

smFISH detection and analysis

Stellaris *Plp* and *Gapdh1* smFISH probes conjugated to Quasar 570 dye (LGC Biosearch Technologies, UK) were designed against the coding region for each gene using the Stellaris RNA FISH probe designer (Ryder et al., 2020; Ryder and Lerit, 2020). smFISH probes were dissolved in nuclease-free water at 25 µM and stored at −20°C before use.

smFISH experiments were performed as previously described (Ryder et al., 2020; Ryder and Lerit, 2020). All the following steps were performed with RNase-free solutions. Embryos were rehydrated and washed first in 0.1% PBST (PBS plus 0.1% Tween-20) and then in wash buffer (WB; 10% formamide and 2× SSC supplemented fresh each experiment with 0.1% Tween-20 and 2 µg/ml nuclease-free BSA). Embryos were then incubated with 100 µl of hybridization buffer [HB; 100 mg/ml dextran sulfate and 10% formamide in 2× SSC supplemented fresh each experiment with 0.1% Tween-20, 2 µg/ml nuclease-free BSA and 10 mM ribonucleoside vanadyl complex (RVC; S1402S; New England Biolabs)] for 10-20 min in a 37°C

Development (2022) 149, dev200426. doi:10.1242/dev.200426

water bath. Embryos were then incubated in 25 µl of HB containing 0.5 µM smFISH probes in a 37°C water bath overnight. Embryos were washed three times for 30 min in prewarmed WB, stained with DAPI (1:1000) for 1 h at room temperature, washed with 0.1% PBST, and mounted with Vectashield mounting medium (H-1000; Vector Laboratories). Slides were stored at 4°C and imaged within 1 week.

smFISH signals were detected and single-molecule normalization was performed as recently described (Ryder et al., 2020; Ryder and Lerit, 2020). Briefly, single-channel .tif raw images were segmented in three dimensions using Python scripts adapted from the Allen Institute for Cell Science Cell Segmenter (Chen et al., 2018 preprint). Each segmented image was compared with the raw image to validate accurate segmentation. RNA objects of ≥50 pixels in segmented images were identified, and object features were extracted, which included surface coordinates. Distances were measured from the surface of each RNA object to the surface of the closest centrosome. We calculated the percentage of total RNA at 0 µm from the centrosome surface and selected 10, 8, 6 and 4 µm as the upper boundaries for the pseudo-cell radius for NC 10, NC 11, NC 12 and NC 13, respectively, based on measuring the centrosome-to-centrosome distances from a set of representative images. Later interphase/prophase embryos were selected by their large, round nuclei and metaphase samples were identified by alignment of condensed chromosomes at the metaphase plate.

Microscopy

Images were acquired on a Nikon Ti-E system fitted with a Yokagawa CSU-X1 spinning disk head, Hamamatsu Orca Flash 4.0 v2 digital complementary metal oxide-semiconductor (CMOS) camera, Perfect Focus system (Nikon), Nikon LU-N4 solid state laser launch (15 mW; 405, 488, 561 and 647 nm) using a Nikon 100×, 1.49 NA Apo TIRF oil-immersion objective. The microscope was powered through Nikon Elements AR software on a 64-bit HP Z440 workstation.

Image analysis

Fiji (National Institutes of Health; Schindelin et al., 2012) was used for all image analysis. To examine nuclear fallout, embryos were stained with anti-Asl antibody to label centrosomes and DAPI to label DNA (Lerit et al., 2015). Areas where centrosomes clustered but were devoid of nuclei were counted as sites of nuclear fallout from genotype-blinded images. To examine CIN, embryos were stained with anti-Asl to label centrosomes, anti-pH3 to label anaphase-lagging chromosomes, and DAPI to label DNA. Anaphase-stage embryos were scored for lagging chromosomes from genotype-blinded images, as defined by laggard chromosome(s) at the spindle equator showing persistent pH3 staining (Fox et al., 2010).

To quantify PLP localization to centrosomes, single-channel PLP .tif raw images were processed as a batch across all genotypes. Blinded images were segmented in three dimensions to display all PLP objects (as segmentation 1), including centriolar and flare zone signals, using Python scripts adapted from the Allen Institute for Cell Science Cell Segmenter (Chen et al., 2018preprint). Each segmented image was compared with the original image to validate accurate segmentation. A second segmentation was performed in order to display only the PLP objects at centrioles (as segmentation 2), and was used as a reference point to identify all PLP objects (segmentation 1) within a centrosome (segmentation 2). Next, all PLP objects were identified, and the raw image total pixel intensity was extracted from a 2 µm region to calculate the intensity of all PLP objects at the centrosome. To validate the accuracy of batch-analysis for PLP quantification, we compared background-subtracted PLP intensity measurements (integrated densities) within 2 µm of the centrosome from n=10 maximum-intensity projected NC 13 WT and recombinant *Plp/+, orb* embryos using manual quantification. Similar results were obtained (Fig. S4), and batch analysis was used subsequently (Fig. 6).

To quantify the number of Cnn fragments per pseudo-cell, single-channel Cnn .tif raw images were segmented as described above. We then used the 3D Objects Counter tool in Fiji to quantify the total number of Cnn fragments in the segmented images, which was then averaged by the total number of nuclei.

Plot profiles of overlapping *Plp* mRNA and GFP-PLP signals were generated using the Plot Profile tool in ImageJ with a single-pixel-wide, 1-µm-long line. Intensities were normalized to the peak fluorescence intensity for each channel and distances were normalized to the peak fluorescence intensity of *Plp* mRNA.

Images were assembled using Fiji, Adobe Photoshop and Adobe Illustrator software to separate or merge channels, crop regions of interest, generate maximum-intensity projections, and adjust brightness and contrast.

RNA immunoprecipitation

RNA immunoprecipitation was performed as previously described (Ryder et al., 2020). Briefly, ovaries were dissected from ∼20 well-fed females and homogenized on ice in 200 µl lysis buffer (50 mM HEPES, pH 7.4, 150 mM NaCl, 2.5 mM $MgCl_2$, 250 mM sucrose and 0.1% Triton X-100) supplemented with 1× EDTA-free protease inhibitor cocktail (Roche, 04693159001), 1 µg/ml Pepstatin A (Sigma-Aldrich, P5318), 1 mM DTT (Sigma-Aldrich, 10197777001), 1 U/µl RNase inhibitor (M0314S; New England Biolabs) and 2 mM RVC. Lysates were cleared by centrifugation at 12,000 rpm (13,523 ***g***), and the supernatant was precleared in 20 µl binding control magnetic beads (bmp-20, ChromoTek) for 30 min at 4°C. Precleared supernatant was then immunoprecipitated with GFP-Trap magnetic agarose beads (gtma-10, ChromoTek) for 2 h at 4°C. Beads were then washed in lysis buffer supplemented with 0.4 mM RVC and resuspended in 100 µl lysis buffer. Twenty-five microliters of bead slurry was reserved and analyzed for protein content by western blotting. RNA was extracted from the remaining 75 µl of beads TRIzol Reagent (15596026, Thermo Fisher Scientific) following treatment with 1 µl TURBO Dnase (AM1907; Thermo Fisher Scientific).

cDNA was synthesized from 500 ng of RNA using Superscript IV Reverse Transcriptase (18091050; Thermo Fisher Scientific) according to the manufacturer's protocol. DNA was amplified by PCR using Phusion High Fidelity DNA Polymerase (M0530L; New England Biolabs) using the following primers: *Plp* Forward, GAAGCCATATCGAAGACACTC; *Plp* Reverse, TGTCAGCCAATAGTCAGTCG; *Gapdh1* Forward, CACCCATTCGTCTGTGTTCG; *Gapdh1* Reverse, CAACAGTGATTCCCGACCAG; *orb* Forward, GTGTGAGACTTTGGACTTGTAGG; *orb* Reverse, GTTTCGATTCGAGGGTGTTCG.

Immunoblotting

Embryo extracts were prepared from ∼10 µl of methanol-fixed embryos. Embryos were rehydrated with 0.1% PBST and homogenized in 150 µl 0.1% PBST using a disposable plastic pestle and cordless motor. Ovarian extracts were similarly prepared from ovaries dissected from ten well-fed females. Thirty microliters of 5× SDS loading buffer was added into the protein extracts, and the samples were boiled at 95°C for 10 min. Extracts were stored at −20°C or immediately resolved on an 7.5% SDS-PAGE pre-cast gel (Bio-Rad, 4568023) and transferred onto a 0.2 µm nitrocellulose membrane (GE Healthcare, 10600001) by wet-transfer in a buffer containing 25 mM Tris-HCl, pH 7.6, 192 mM glycine, 10% methanol and 0.02% SDS. Membranes were blocked for 1 h at room temperature in 5% dry milk diluted in TBST (Tris-based saline with 0.05% Tween-20), washed well with TBST, and incubated overnight at 4°C with primary antibodies. After washing with TBST, membranes were incubated for 1.5 h in secondary antibodies diluted 1:5000 in TBST. Bands were visualized with Clarity ECL substrate (Bio-Rad, 1705061) on a Bio-Rad ChemiDoc imaging system.

The following primary antibodies were used: rabbit anti-PLP (1:4000, gift from N. Rusan, National Institutes of Health), mouse anti-Khc SUK 4 (1:200, DSHB; J. M. Scholey, University of Colorado, USA), guinea pig anti-Asl (1:10,000, gift from G. Rogers, University of Arizona, USA), mouse anti-β-Tubulin E7 (1:1000, DSHB; M. Klymkowsky, University of Colorado, USA), mouse anti-Orb 4H8 (1:100, DHSB; P. Schedl, Princeton University, USA). Secondary antibody was goat anti-mouse HRP (1:5000, Thermo Fisher Scientific, 31430). Densitometry was measured in Adobe Photoshop and protein levels were normalized to the loading control.

qRT-PCR

RNA was extracted from ∼2-5 mg of dechorionated 0- to 2 h-old embryos or ovaries dissected from five well-fed females per biological replicate using TRIzol Reagent (15596026, Thermo Fisher Scientific) and treated with1 µl

Development (2022) 149, dev200426. doi:10.1242/dev.200426

TURBO Dnase (2 U/µl, AM1907, Thermo Fisher Scientific) prior to RT-PCR. Five-hundred nanograms of RNA was reverse transcribed to cDNA with Superscript IV Reverse Transcriptase following the manufacturer's protocol. qPCR was performed on a Bio-Rad CFX96 Real-time system with iTaq Universal SYBR Green Supermix (1725121, Bio-Rad). Values were normalized to *RpL32* (*rp49*) expression levels. Ct values from the qPCR results were analyzed and the relative expression levels for each condition were calculated using Microsoft Excel. Three biological replicates and three technical replicates were performed on a single 96-well plate.

The primers used in this study were: *rp49* Forward, CATACAGGCC-CAAGATCGTG; *rp49* Reverse, ACAGCTTAGCATATCGATCCG; *Plp* Forward, CGCAGCAAGGAGGAGATAAC; *Plp* Reverse, TCAGCCTG-CAGTTTGTTCAC; Plp^{RM} Forward, TGTCCCAGTATTTTGATTGGT; Plp^{RM} Reverse, GTCCAGTGAATTCTCACCCT.

PAT assay

Two micrograms of 0- to 2-h-old embryos were harvested and RNA was extracted with TRIzol Reagent (15596026, Thermo Fisher Scientific). The PAT test was conducted following the manufacturer's protocol (Thermo Fisher Scientific, PAT kit, 76455). Briefly, 3 µg of RNA was digested with Turbo dNase (2 U/µl, AM1907, Thermo Fisher Scientific), then 500 ng of dNase-digested RNA was tagged with G/I tails in a 10 µl reaction, and 5 µl of G/I-tailed RNAs were reverse transcribed using a universal primer complementary to the G/I tails to synthesize cDNA in a 20 µl reaction. Twenty microliters of cDNA was diluted 1:1 into nuclease-free water, and 10 µl was then used to amplify PAT products using a *Plp*-specific forward primer and a universal reverse primer complementary to the G/I tails in a 50 µl reaction using a two-step PCR protocol and Taq polymerase, as provided by the manufacturer. To amplify long or short *Plp* 3′-UTRs, 2 µl of diluted cDNA was used as template using the indicated primers in a 50 µl reaction using Phusion High Fidelity DNA Polymerase (M0530L; New England Biolabs). Fifteen microliters of amplified DNA was used for EcoRI and BmrI restriction enzyme digestion (New England Biolabs). DNA products were separated by gel electrophoresis on a 3% agarose gel. The primer PAT_{Rev} was part of the PAT kit and is proprietary to the manufacturer. The primers we designed that were used in this study were: Plp_{Rev1}, CGAATGTGAAATAAATTTGGTT; Plp_{Rev2}, CTACTGCTTTC-GATACCTTTTT; Plp_{Fw}, ACCTGTACCATTTCCCCTCA.

Statistical methods

Data were plotted and statistical analysis was performed using GraphPad Prism software. To calculate significance, distribution normality was first confirmed with a D'Agnostino and Pearson normality test. Data were then analyzed by unpaired *t*-test or one-way ANOVA test or a χ^2 test and are displayed as mean±s.d. Data shown are representative results from at least two independent experiments.

Acknowledgements

We thank Drs Nasser Rusan, Greg Rogers and Timothy Megraw for gifts of reagents; Drs Elizabeth Gavis, Amanda Norvell and Martine Simonelig for advice about the PAT assay; Dr Pearl Ryder for computational assistance; Ms Beverly Robinson for technical advice on ontological analysis; and Mr Jovan Brockett for embryo collections. We are grateful to Drs Paul Schedl, Gary Bassell and Guohong Li for constructive feedback on the manuscript.

Competing interests

The authors declare no competing or financial interests.

Author contributions

Conceptualization: D.A.L.; Methodology: J.F.; Software: J.F.; Validation: J.F.; Formal analysis: J.F.; Investigation: J.F.; Writing - original draft: J.F., D.A.L.; Writing - review & editing: J.F., D.A.L.; Visualization: J.F.; Supervision: D.A.L.; Project administration: J.F., D.A.L.; Funding acquisition: J.F., D.A.L.

Funding

This work was supported by the National Institutes of Health [R01GM138544 to D.A.L. and K99GM143517 to J.F.] and the American Heart Association [20POST35210023 to J.F.]. Deposited in PMC for release after 12 months.

Data availability

Uncropped gels and blots are available to view on Figshare: https://doi.org/10.6084/m9.figshare.16900417.v1; https://doi.org/10.6084/m9.figshare.16900423.v1; https://doi.org/10.6084/m9.figshare.16900471.v4; https://doi.org/10.6084/m9.figshare.16900429.v4.

Peer review history

The peer review history is available online at https://journals.biologists.com/dev/article-lookup/doi/10.1242/dev.200426.

References

Barkoff, A. F., Dickson, K. S., Gray, N. K. and Wickens, M. (2000). Translational control of cyclin B1 mRNA during meiotic maturation: coordinated repression and cytoplasmic polyadenylation. *Dev. Biol.* **220**, 97-109. doi:10.1006/dbio.2000.9613

Benoit, P., Papin, C., Kwak, J. E., Wickens, M. and Simonelig, M. (2008). PAP- and GLD-2-type poly(A) polymerases are required sequentially in cytoplasmic polyadenylation and oogenesis in Drosophila. *Development* **135**, 1969-1979. doi:10.1242/dev.021444

Blower, M. D., Feric, E., Weis, K. and Heald, R. (2007). Genome-wide analysis demonstrates conserved localization of messenger RNAs to mitotic microtubules. *J. Cell Biol.* **179**, 1365-1373. doi:10.1083/jcb.200705163

Brizuela, B. J., Elfring, L., Ballard, J., Tamkun, J. W. and Kennison, J. A. (1994). Genetic analysis of the brahma gene of Drosophila melanogaster and polytene chromosome subdivisions 72AB. *Genetics* **137**, 803-813. doi:10.1093/genetics/137.3.803

Burns, D. M. and Richter, J. D. (2008). CPEB regulation of human cellular senescence, energy metabolism, and p53 mRNA translation. *Genes Dev.* **22**, 3449-3460. doi:10.1101/gad.1697808

Burns, D. M., D'ambrogio, A., Nottrott, S. and Richter, J. D. (2011). CPEB and two poly(A) polymerases control miR-122 stability and p53 mRNA translation. *Nature* **473**, 105. doi:10.1038/nature09908

Buxbaum, A. R., Haimovich, G. and Singer, R. H. (2015). In the right place at the right time: visualizing and understanding mRNA localization. *Nat. Rev. Mol. Cell Biol.* **16**, 95. doi:10.1038/nrm3918

Cao, Q. and Richter, J. D. (2002). Dissolution of the maskin–eIF4E complex by cytoplasmic polyadenylation and poly(A)-binding protein controls cyclin B1 mRNA translation and oocyte maturation. *EMBO J.* **21**, 3852-3862. doi:10.1093/emboj/cdf353

Castagnetti, S. and Ephrussi, A. (2003). Orb and a long poly(A) tail are required for efficient oskar; translation at the posterior pole of the Drosophila oocyte. *Development* **130**, 835. doi:10.1242/dev.00309

Chang, J. S., Tan, L. and Schedl, P. (1999). The Drosophila CPEB homolog, Orb, is required for oskar protein expression in oocytes. *Dev. Biol.* **215**, 91-106. doi:10.1006/dbio.1999.9444

Chang, J. S., Tan, L., Wolf, M. R. and Schedl, P. (2001). Functioning of the Drosophila orb gene in gurken mRNA localization and translation. *Development* **128**, 3169. doi:10.1242/dev.128.16.3169

Chen, C.-T., Hehnly, H., Yu, Q., Farkas, D., Zheng, G., Redick, S. D., Hung, H.-F., Samtani, R., Jurczyk, A., Akbarian, S. et al. (2014). A unique set of centrosome proteins requires pericentrin for spindle-pole localization and spindle orientation. *Curr. Biol.* **24**, 2327-2334. doi:10.1016/j.cub.2014.08.029

Chen, J., Ding, L., Viana, M. P., Lee, H. W., Sluezwski, M. F., Morris, B., Hendershott, M. C., Yang, R., Mueller, I. A. and Rafelski, S. M. (2018). The Allen Cell Structure Segmenter: a new open source toolkit for segmenting 3D intracellular structures in fluorescence microscopy images. *bioRxiv*, 491035. doi:10.1101/491035

Choi, K. M., Barash, I. and Rhoads, R. E. (2004). Insulin and prolactin synergistically stimulate β-casein messenger ribonucleic acid translation by cytoplasmic polyadenylation. *Mol. Endocrinol.* **18**, 1670-1686. doi:10.1210/me.2003-0483

Chou, T.-B. and Perrimon, N. (1996). The autosomal FLP-DFS technique for generating germline mosaics in Drosophila melanogaster. *Genetics* **144**, 1673. doi:10.1093/genetics/144.4.1673

Chouaib, R., Safieddine, A., Pichon, X., Imbert, A., Kwon, O. S., Samacoits, A., Traboulsi, A.-M., Robert, M.-C., Tsanov, N., Coleno, E. et al. (2020). A dual protein-mRNA localization screen reveals compartmentalized translation and widespread co-translational RNA targeting. *Dev. Cell* **54**, 773-791.e5 doi:10.1016/j.devcel.2020.07.010

Christerson, L. B. and Mckearin, D. M. (1994). orb is required for anteroposterior and dorsoventral patterning during Drosophila oogenesis. *Genes Dev.* **8**, 614-628. doi:10.1101/gad.8.5.614

Cody, N. A. L., Iampietro, C. and Lécuyer, E. (2013). The many functions of mRNA localization during normal development and disease: from pillar to post. *Wiley Interdiscipl. Rev. Dev. Biol.* **2**, 781-796. doi:10.1002/wdev.113

Coll, O., Villalba, A., Bussotti, G., Notredame, C. and Gebauer, F. (2010). A novel, noncanonical mechanism of cytoplasmic polyadenylation operates in Drosophila embryogenesis. *Genes Dev.* **24**, 129-134. doi:10.1101/gad.568610

Conduit, P. T., Richens, J. H., Wainman, A., Holder, J., Vicente, C. C., Pratt, M. B., Dix, C. I., Novak, Z. A., Dobbie, I. M., Schermelleh, L. et al. (2014).

A molecular mechanism of mitotic centrosome assembly in Drosophila. *eLife* **3**, e03399. doi:10.7554/eLife.03399

Costa, A., Wang, Y., Dockendorff, T. C., Erdjument-Bromage, H., Tempst, P., Schedl, P. and Jongens, T. A. (2005). The Drosophila Fragile X protein functions as a negative regulator in the orb autoregulatory pathway. *Dev. Cell* **8**, 331-342. doi:10.1016/j.devcel.2005.01.011

Das, S., Vera, M., Gandin, V., Singer, R. H. and Tutucci, E. (2021). Intracellular mRNA transport and localized translation. *Nat. Rev. Mol. Cell Biol.* **22**, 483-504. doi:10.1038/s41580-021-00356-8

Davidson, A., Parton, R. M., Rabouille, C., Weil, T. T. and Davis, I. (2016). Localized translation of gurken/TGF-α mRNA during axis specification is controlled by access to Orb/CPEB on processing bodies. *Cell Rep.* **14**, 2451-2462. doi:10.1016/j.celrep.2016.02.038

Delaval, B. and Doxsey, S. J. (2010). Pericentrin in cellular function and disease. *J. Cell Biol.* **188**, 181. doi:10.1083/jcb.200908114

Dictenberg, J. B., Zimmerman, W., Sparks, C. A., Young, A., Vidair, C., Zheng, Y., Carrington, W., Fay, F. S. and Doxsey, S. J. (1998). Pericentrin and γ-tubulin form a protein complex and are organized into a novel lattice at the centrosome. *J. Cell Biol.* **141**, 163-174. doi:10.1083/jcb.141.1.163

Dobbelaere, J., Josué, F., Suijkerbuijk, S., Baum, B., Tapon, N. and Raff, J. (2008). A genome-wide RNAi screen to dissect centriole duplication and centrosome maturation in Drosophila. *PLoS Biol.* **6**, e224. doi:10.1371/journal.pbio.0060224

Dockendorff, T. C., Su, H. S., Mcbride, S. M. J., Yang, Z., Choi, C. H., Siwicki, K. K., Sehgal, A. and Jongens, T. A. (2002). Drosophila lacking dfmr1 activity show defects in circadian output and fail to maintain courtship interest. *Neuron* **34**, 973-984. doi:10.1016/S0896-6273(02)00724-9

Eichhorn, S. W., Subtelny, A. O., Kronja, I., Kwasnieski, J. C., Orr-Weaver, T. L. and Bartel, D. P. (2016). mRNA poly(A)-tail changes specified by deadenylation broadly reshape translation in Drosophila oocytes and early embryos. *eLife* **5**, e16955. doi:10.7554/eLife.16955

Eliscovich, C., Peset, I., Vernos, I. and Méndez, R. (2008). Spindle-localized CPE-mediated translation controls meiotic chromosome segregation. *Nat. Cell Biol.* **10**, 858-865. doi:10.1038/ncb1746

Fang, J. and Lerit, D. A. (2020). Drosophila pericentrin-like protein promotes the formation of primordial germ cells. *Genesis* **58**, e23347. doi:10.1002/dvg.23347

Foe, V. E. and Alberts, B. M. (1983). Studies of nuclear and cytoplasmic behaviour during the five mitotic cycles that precede gastrulation in Drosophila embryogenesis. *J. Cell Sci.* **61**, 31. doi:10.1242/jcs.61.1.31

Fox, C. A., Sheets, M. D. and Wickens, M. P. (1989). Poly(A) addition during maturation of frog oocytes: distinct nuclear and cytoplasmic activities and regulation by the sequence UUUUUAU. *Genes Dev.* **3**, 2151-2162. doi:10.1101/gad.3.12b.2151

Fox, D. T., Gall, J. G. and Spradling, A. C. (2010). Error-prone polyploid mitosis during normal Drosophila development. *Genes Dev.* **24**, 2294-2302. doi:10.1101/gad.1952710

Fu, J. and Glover, D. M. (2012). Structured illumination of the interface between centriole and peri-centriolar material. *Open Biology* **2**, 120104. doi:10.1098/rsob.120104

Galati, D. F., Sullivan, K. D., Pham, A. T., Espinosa, J. M. and Pearson, C. G. (2018). Trisomy 21 represses cilia formation and function. *Dev. Cell* **46**, 641-650.e6. doi:10.1016/j.devcel.2018.07.008

Galletta, B. J., Guillen, R. X., Fagerstrom, C. J., Brownlee, C. W., Lerit, D. A., Megraw, T. L., Rogers, G. C., Rusan, N. M. and Bettencourt-Dias, M. (2014). Drosophila pericentrin requires interaction with calmodulin for its function at centrosomes and neuronal basal bodies but not at sperm basal bodies. *Mol. Biol. Cell* **25**, 2682-2694. doi:10.1091/mbc.e13-10-0617

Galletta, B. J., Ortega, J. M., Smith, S. L., Fagerstrom, C. J., Fear, J. M., Mahadevaraju, S., Oliver, B. and Rusan, N. M. (2020). Sperm head-tail linkage requires restriction of pericentriolar material to the proximal centriole end. *Dev. Cell* **53**, 86-101.e7. doi:10.1016/j.devcel.2020.02.006

Goldman-Huertas, B., Mitchell, R. F., Lapoint, R. T., Faucher, C. P., Hildebrand, J. G. and Whiteman, N. K. (2015). Evolution of herbivory in Drosophilidae linked to loss of behaviors, antennal responses, odorant receptors, and ancestral diet. *Proc. Natl Acad. Sci. USA* **112**, 3026-3031. doi:10.1073/pnas.1424656112

Gould, R. R. and Borisy, G. G. (1977). The pericentriolar material in Chinese hamster ovary cells nucleates microtubule formation. *J. Cell Biol.* **73**, 601-615. doi:10.1083/jcb.73.3.601

Graveley, B. R., Brooks, A. N., Carlson, J. W., Duff, M. O., Landolin, J. M., Yang, L., Artieri, C. G., Van Baren, M. J., Boley, N., Booth, B. W. et al. (2011). The developmental transcriptome of Drosophila melanogaster. *Nature* **471**, 473-479. doi:10.1038/nature09715

Groisman, I., Huang, Y.-S., Mendez, R., Cao, Q., Theurkauf, W. and Richter, J. D. (2000). CPEB, Maskin, and Cyclin B1 mRNA at the mitotic apparatus: implications for local translational control of cell division. *Cell* **103**, 435-447. doi:10.1016/S0092-8674(00)00135-5

Groisman, I., Jung, M.-Y., Sarkissian, M., Cao, Q. and Richter, J. D. (2002). Translational control of the embryonic cell cycle. *Cell* **109**, 473-483. doi:10.1016/S0092-8674(02)00733-X

Groisman, I., Ivshina, M., Marin, V., Kennedy, N. J., Davis, R. J. and Richter, J. D. (2006). Control of cellular senescence by CPEB. *Genes Dev.* **20**, 2701-2712. doi:10.1101/gad.1438906

Hafer, N., Xu, S., Bhat, K. M. and Schedl, P. (2011). The Drosophila CPEB protein Orb2 has a novel expression pattern and is important for asymmetric cell division and nervous system function. *Genetics* **189**, 907-921. doi:10.1534/genetics.110.123646

Hake, L. E. and Richter, J. D. (1994). CPEB is a specificity factor that mediates cytoplasmic polyadenylation during Xenopus oocyte maturation. *Cell* **79**, 617-627. doi:10.1016/0092-8674(94)90547-9

Haren, L., Stearns, T. and Lüders, J. (2009). Plk1-dependent recruitment of γ-tubulin complexes to mitotic centrosomes involves multiple PCM Components. *PLoS ONE* **4**, e5976. doi:10.1371/journal.pone.0005976

Hodgman, R., Tay, J., Mendez, R. and Richter, J. D. (2001). CPEB phosphorylation and cytoplasmic polyadenylation are catalyzed by the kinase IAK1/Eg2 in maturing mouse oocytes. *Development* **128**, 2815-2822. doi:10.1242/dev.128.14.2815

Johnstone, O. and Lasko, P. (2001). Translational regulation and RNA localization in Drosophila oocytes and embryos. *Annu. Rev. Genet.* **35**, 365-406. doi:10.1146/annurev.genet.35.102401.090756

Jurczyk, A., Gromley, A., Redick, S., Agustin, J. S., Witman, G., Pazour, G. J., Peters, D. J. M. and Doxsey, S. (2004). Pericentrin forms a complex with intraflagellar transport proteins and polycystin-2 and is required for primary cilia assembly. *J. Cell Biol.* **166**, 637. doi:10.1083/jcb.200405023

Keleman, K., Krüttner, S., Alenius, M. and Dickson, B. J. (2007). Function of the Drosophila CPEB protein Orb2 in long-term courtship memory. *Nat. Neurosci.* **10**, 1587-1593. doi:10.1038/nn1996

Kent, W. J., Sugnet, C. W., Furey, T. S., Roskin, K. M., Pringle, T. H., Zahler, A. M. and Haussler, D. (2002). The Human Genome Browser at UCSC. *Genome Res.* **12**, 996-1006. doi:10.1101/gr.229102

Khodjakov, A. and Rieder, C. L. (1999). The sudden recruitment of γ-tubulin to the centrosome at the onset of mitosis and its dynamic exchange throughout the cell cycle, do not require microtubules. *J. Cell Biol.* **146**, 585-596. doi:10.1083/jcb.146.3.585

Kim, J. H. and Richter, J. D. (2007). RINGO/cdk1 and CPEB mediate poly(A) tail stabilization and translational regulation by ePAB. *Genes Dev.* **21**, 2571-2579. doi:10.1101/gad.1593007

Kim, J., Lee, K. and Rhee, K. (2015). PLK1 regulation of PCNT cleavage ensures fidelity of centriole separation during mitotic exit. *Nat. Commun.* **6**, 10076. doi:10.1038/ncomms10076

Kislauskis, E. H., Zhu, X. and Singer, R. H. (1994). Sequences responsible for intracellular localization of beta-actin messenger RNA also affect cell phenotype. *J. Cell Biol.* **127**, 441-451. doi:10.1083/jcb.127.2.441

Kwon, O. S., Mishra, R., Safieddine, A., Coleno, E., Alasseur, Q., Faucourt, M., Barbosa, I., Bertrand, E., Spassky, N. and Le Hir, H. (2021). Exon junction complex dependent mRNA localization is linked to centrosome organization during ciliogenesis. *Nat. Commun.* **12**, 1351. doi:10.1038/s41467-021-21590-w

Lantz, V., Ambrosio, L. and Schedl, P. (1992). The Drosophila orb gene is predicted to encode sex-specific germline RNA-binding proteins and has localized transcripts in ovaries and early embryos. *Development* **115**, 75. doi:10.1242/dev.115.1.75

Lantz, V., Chang, J. S., Horabin, J. I., Bopp, D. and Schedl, P. (1994). The Drosophila orb RNA-binding protein is required for the formation of the egg chamber and establishment of polarity. *Genes Dev.* **8**, 598-613. doi:10.1101/gad.8.5.598

Larkin, A., Marygold, S. J., Antonazzo, G., Attrill, H., Dos Santos, G., Garapati, P. V., Goodman, J. L., Gramates, L. S., Millburn, G., Strelets, V. B. et al. (2021). FlyBase: updates to the Drosophila melanogaster knowledge base. *Nucleic Acids Res.* **49**, D899-D907. doi:10.1093/nar/gkaa1026

Lawo, S., Hasegan, M., Gupta, G. D. and Pelletier, L. (2012). Subdiffraction imaging of centrosomes reveals higher-order organizational features of pericentriolar material. *Nat. Cell Biol.* **14**, 1148. doi:10.1038/ncb2591

Lécuyer, E., Yoshida, H., Parthasarathy, N., Alm, C., Babak, T., Cerovina, T., Hughes, T. R., Tomancak, P. and Krause, H. M. (2007). Global analysis of mRNA localization reveals a prominent role in organizing cellular architecture and function. *Cell* **131**, 174-187. doi:10.1016/j.cell.2007.08.003

Lee, K. and Rhee, K. (2011). PLK1 phosphorylation of pericentrin initiates centrosome maturation at the onset of mitosis. *J. Cell Biol.* **195**, 1093. doi:10.1083/jcb.201106093

Legnini, I., Alles, J., Karaiskos, N., Ayoub, S. and Rajewsky, N. (2019). FLAM-seq: full-length mRNA sequencing reveals principles of poly(A) tail length control. *Nat. Methods* **16**, 879-886. doi:10.1038/s41592-019-0503-y

Lerit, D. A. and Rusan, N. M. (2013). PLP inhibits the activity of interphase centrosomes to ensure their proper segregation in stem cells. *J. Cell Biol.* **202**, 1013. doi:10.1083/jcb.201303141

Lerit, D. A., Jordan, H. A., Poulton, J. S., Fagerstrom, C. J., Galletta, B. J., Peifer, M. and Rusan, N. M. (2015). Interphase centrosome organization by the PLP-Cnn scaffold is required for centrosome function. *J. Cell Biol.* **210**, 79-97. doi:10.1083/jcb.201503117

Lerit, D. A., Shebelut, C. W., Lawlor, K. J., Rusan, N. M., Gavis, E. R., Schedl, P. and Deshpande, G. (2017). Germ cell-less promotes centrosome segregation to induce germ cell formation. *Cell Rep.* **18**, 831-839. doi:10.1016/j.celrep.2016.12.074

Lim, J., Lee, M., Son, A., Chang, H. and Kim, V. N. (2016). mTAIL-seq reveals dynamic poly(A) tail regulation in oocyte-to-embryo development. *Genes Dev.* **30**, 1671-1682. doi:10.1101/gad.284802.116

Madeira, F., Park, Y. M., Lee, J., Buso, N., Gur, T., Madhusoodanan, N., Basutkar, P., Tivey, A. R. N., Potter, S. C., Finn, R. D. et al. (2019). The EMBL-EBI search and sequence analysis tools APIs in 2019. *Nucleic Acids Res.* **47**, W636-W641. doi:10.1093/nar/gkz268

Mansfield, J. H., Wilhelm, J. E. and Hazelrigg, T. (2002). Ypsilon Schachtel, a Drosophila Y-box protein, acts antagonistically to Orb in the oskar mRNA localization and translation pathway. *Development* **129**, 197. doi:10.1242/dev.129.1.197

Martinez-Campos, M., Basto, R., Baker, J., Kernan, M. and Raff, J. W. (2004). The Drosophila pericentrin-like protein is essential for cilia/flagella function, but appears to be dispensable for mitosis. *J. Cell Biol.* **165**, 673. doi:10.1083/jcb.200402130

Mastushita-Sakai, T., White-Grindley, E., Samuelson, J., Seidel, C. and Si, K. (2010). Drosophila Orb2 targets genes involved in neuronal growth, synapse formation, and protein turnover. *Proc. Natl. Acad. Sci. USA* **107**, 11987. doi:10.1073/pnas.1004433107

Mcgrew, L. L. and Richter, J. D. (1990). Translational control by cytoplasmic polyadenylation during Xenopus oocyte maturation: characterization of cis and trans elements and regulation by cyclin/MPF. *EMBO J.* **9**, 3743-3751. doi:10.1002/j.1460-2075.1990.tb07587.x

Megraw, T. L., Kilaru, S., Turner, F. R. and Kaufman, T. C. (2002). The centrosome is a dynamic structure that ejects PCM flares. *J. Cell Sci.* **115**, 4707. doi:10.1242/jcs.00134

Mendez, R. and Richter, J. D. (2001). Translational control by CPEB: a means to the end. *Nat. Rev. Mol. Cell Biol.* **2**, 521-529. doi:10.1038/35080081

Mendez, R., Hake, L. E., Andresson, T., Littlepage, L. E., Ruderman, J. V. and Richter, J. D. (2000a). Phosphorylation of CPE binding factor by Eg2 regulates translation of c-mos mRNA. *Nature* **404**, 302-307. doi:10.1038/35005126

Mendez, R., Murthy, K. G. K., Ryan, K., Manley, J. L. and Richter, J. D. (2000b). Phosphorylation of CPEB by Eg2 mediates the recruitment of CPSF into an active cytoplasmic polyadenylation complex. *Mol. Cell* **6**, 1253-1259. doi:10.1016/S1097-2765(00)00121-0

Mennella, V., Keszthelyi, B., Mcdonald, K. L., Chhun, B., Kan, F., Rogers, G. C., Huang, B. and Agard, D. A. (2012). Subdiffraction-resolution fluorescence microscopy reveals a domain of the centrosome critical for pericentriolar material organization. *Nat. Cell Biol.* **14**, 1159-1168. doi:10.1038/ncb2597

Mi, H., Ebert, D., Muruganujan, A., Mills, C., Albou, L.-P., Mushayamaha, T. and Thomas, P. D. (2021). PANTHER version 16: a revised family classification, tree-based classification tool, enhancer regions and extensive API. *Nucleic Acids Res.* **49**, D394-D403. doi:10.1093/nar/gkaa1106

Nagaoka, K., Udagawa, T. and Richter, J. D. (2012). CPEB-mediated ZO-1 mRNA localization is required for epithelial tight-junction assembly and cell polarity. *Nat. Commun.* **3**, 675. doi:10.1038/ncomms1678

Nagarkar-Jaiswal, S., Lee, P.-T., Campbell, M. E., Chen, K., Anguiano-Zarate, S., Cantu Gutierrez, M., Busby, T., Lin, W.-W., He, Y., Schulze, K. L. et al. (2015). A library of MiMICs allows tagging of genes and reversible, spatial and temporal knockdown of proteins in Drosophila. *eLife* **4**, e05338. doi:10.7554/eLife.05338.023

Norvell, A., Wong, J., Randolph, K. and Thompson, L. (2015). Wispy and Orb cooperate in the cytoplasmic polyadenylation of localized gurken mRNA. *Dev. Dyn.* **244**, 1276-1285. doi:10.1002/dvdy.24311

Novoa, I., Gallego, J., Ferreira, P. G. and Mendez, R. (2010). Mitotic cell-cycle progression is regulated by CPEB1 and CPEB4-dependent translational control. *Nat. Cell Biol.* **12**, 447-456. doi:10.1038/ncb2046

Palazzo, R. E., Vogel, J. M., Schnackenberg, B. J., Hull, D. R. and Wu, X. (1999). Centrosome maturation. *Curr. Top. Dev. Biol* **49**, 449-470. doi:10.1016/s0070-2153(99)49021-0

Pandey, R., Heidmann, S. and Lehner, C. F. (2005). Epithelial re-organization and dynamics of progression through mitosis in Drosophila separase complex mutants. *J. Cell Sci.* **118**, 733-742. doi:10.1242/jcs.01663

Pascual, R., Segura-Morales, C., Omerzu, M., Bellora, N., Belloc, E., Castellazzi, C. L., Reina, O., Eyras, E., Maurice, M. M., Millanes-Romero, A. et al. (2021). mRNA spindle localization and mitotic translational regulation by CPEB1 and CPEB4. *RNA* **27**, 291-302. doi:10.1261/rna.077552.120

Passmore, L. A. and Coller, J. (2021). Roles of mRNA poly(A) tails in regulation of eukaryotic gene expression. *Nat. Rev. Mol. Cell Biol.* **23**, 93-106. doi:10.1038/s41580-021-00417-y

Piqué, M., López, J. M., Foissac, S., Guigó, R. and Méndez, R. (2008). A combinatorial code for CPE-mediated translational control. *Cell* **132**, 434-448. doi:10.1016/j.cell.2007.12.038

Rangan, P., Degennaro, M., Jaime-Bustamante, K., Coux, R.-X., Martinho, R. G. and Lehmann, R. (2009). Temporal and spatial control of germ-plasm RNAs. *Curr. Biol.* **19**, 72-77. doi:10.1016/j.cub.2008.11.066

Rauch, A., Thiel, C. T., Schindler, D., Wick, U., Crow, Y. J., Ekici, A. B., Van Essen, A. J., Goecke, T. O., Al-Gazali, L., Chrzanowska, K. H. et al. (2008). Mutations in the Pericentrin (PCNT) gene cause primordial dwarfism. *Science* **319**, 816. doi:10.1126/science.1151174

Richens, J. H., Barros, T. P., Lucas, E. P., Peel, N., Pinto, D. M. S., Wainman, A. and Raff, J. W. (2015). The Drosophila Pericentrin-like-protein (PLP) cooperates with Cnn to maintain the integrity of the outer PCM. *Biol. Open* **4**, 1052. doi:10.1242/bio.012914

Rojas-Ríos, P., Chartier, A., Pierson, S., Séverac, D., Dantec, C., Busseau, I. and Simonelig, M. (2015). Translational control of autophagy by orb in the Drosophila germline. *Dev. Cell* **35**, 622-631. doi:10.1016/j.devcel.2015.11.003

Roque, H., Saurya, S., Pratt, M. B., Johnson, E. and Raff, J. W. (2018). Drosophila PLP assembles pericentriolar clouds that promote centriole stability, cohesion and MT nucleation. *PLoS Genet.* **14**, e1007198. doi:10.1371/journal.pgen.1007198

Rothwell, W. F. and Sullivan, W. (1999). The centrosome in early Drosophila embryogenesis. In *Current Topics in Developmental Biology* (ed. R. E. Palazzo and G. P. Schatten). Academic Press.

Rothwell, W. F. and Sullivan, W. (2007). Fixation of Drosophila embryos. *CSH Protoc.* **2007**, 409-447. doi:10.1101/pdb.prot4827

Rothwell, W. F., Fogarty, P., Field, C. M. and Sullivan, W. (1998). Nuclear-fallout, a Drosophila protein that cycles from the cytoplasm to the centrosomes, regulates cortical microfilament organization. *Development* **125**, 1295-1303. doi:10.1242/dev.125.7.1295

Ryder, P. V. and Lerit, D. A. (2018). RNA localization regulates diverse and dynamic cellular processes. *Traffic* **19**, 496-502. doi:10.1111/tra.12571

Ryder, P. V. and Lerit, D. A. (2020). Quantitative analysis of subcellular distributions with an open-source, object-based tool. *Biol. Open* **9**, bio.055228. doi:10.1242/bio.055228

Ryder, P. V., Fang, J. and Lerit, D. A. (2020). centrocortin RNA localization to centrosomes is regulated by FMRP and facilitates error-free mitosis. *J. Cell Biol.* **219**, e202004101. doi:10.1083/jcb.202004101

Safieddine, A., Coleno, E., Salloum, S., Imbert, A., Traboulsi, A.-M., Kwon, O. S., Lionneton, F., Georget, V., Robert, M.-C., Gostan, T. et al. (2021). A choreography of centrosomal mRNAs reveals a conserved localization mechanism involving active polysome transport. *Nat. Commun.* **12**, 1352. doi:10.1038/s41467-021-21585-7

Schindelin, J., Arganda-Carreras, I., Frise, E., Kaynig, V., Longair, M., Pietzsch, T., Preibisch, S., Rueden, C., Saalfeld, S., Schmid, B. et al. (2012). Fiji: an open-source platform for biological-image analysis. *Nat. Methods* **9**, 676-682. doi:10.1038/nmeth.2019

Sepulveda, G., Antkowiak, M., Brust-Mascher, I., Mahe, K., Ou, T., Castro, N. M., Christensen, L. N., Cheung, L., Jiang, X., Yoon, D. et al. (2018). Co-translational protein targeting facilitates centrosomal recruitment of PCNT during centrosome maturation in vertebrates. *eLife* **7**, e34959. doi:10.7554/eLife.34959

Sharp, J. A., Plant, J. J., Ohsumi, T. K., Borowsky, M. and Blower, M. D. (2011). Functional analysis of the microtubule-interacting transcriptome. *Mol. Biol. Cell* **22**, 4312-4323. doi:10.1091/mbc.e11-07-0629

Sonnen, K. F., Schermelleh, L., Leonhardt, H. and Nigg, E. A. (2012). 3D-structured illumination microscopy provides novel insight into architecture of human centrosomes. *Biol. Open* **1**, 965-976. doi:10.1242/bio.20122337

Spradling, A. C., Stern, D., Beaton, A., Rhem, E. J., Laverty, T., Mozden, N., Misra, S. and Rubin, G. M. (1999). The Berkeley Drosophila Genome Project Gene Disruption Project: single P-element insertions mutating 25% of vital Drosophila genes. *Genetics* **153**, 135. doi:10.1093/genetics/153.1.135

Stebbins-Boaz, B., Hake, L. E. and Richter, J. D. (1996). CPEB controls the cytoplasmic polyadenylation of cyclin, Cdk2 and c-mos mRNAs and is necessary for oocyte maturation in Xenopus. *EMBO J.* **15**, 2582-2592. doi:10.1002/j.1460-2075.1996.tb00616.x

Stepien, B. K., Oppitz, C., Gerlach, D., Dag, U., Novatchkova, M., Krüttner, S., Stark, A. and Keleman, K. (2016). RNA-binding profiles of Drosophila CPEB proteins Orb and Orb2. *Proc. Natl. Acad. Sci. USA* **113**, E7030-E7038. doi:10.1073/pnas.1603715113

Subtelny, A. O., Eichhorn, S. W., Chen, G. R., Sive, H. and Bartel, D. P. (2014). Poly(A)-tail profiling reveals an embryonic switch in translational control. *Nature* **508**, 66-71. doi:10.1038/nature13007

Sullivan, W., Fogarty, P. and Theurkauf, W. (1993). Mutations affecting the cytoskeletal organization of syncytial Drosophila embryos. *Development* **118**, 1245-1254. doi:10.1242/dev.118.4.1245

Tadros, W. and Lipshitz, H. D. (2009). The maternal-to-zygotic transition: a play in two acts. *Development* **136**, 3033. doi:10.1242/dev.033183

Tan, L., Chang, J. S., Costa, A. and Schedl, P. (2001). An autoregulatory feedback loop directs the localized expression of the Drosophila CPEB protein Orb in the developing oocyte. *Development* **128**, 1159. doi:10.1242/dev.128.7.1159

Varmark, H., Llamazares, S., Rebollo, E., Lange, B., Reina, J., Schwarz, H. and Gonzalez, C. (2007). Asterless is a centriolar protein required for centrosome function and embryo development in Drosophila. *Curr. Biol.* **17**, 1735-1745. doi:10.1016/j.cub.2007.09.031

Vertii, A., Hehnly, H. and Doxsey, S. (2016). The centrosome, a multitalented renaissance organelle. *Cold Spring Harbor Perspect. Biol.* **8**, a025049. doi:10.1101/cshperspect.a025049

Vitre, B. D. and Cleveland, D. W. (2012). Centrosomes, chromosome instability (CIN) and aneuploidy. *Curr. Opin. Cell Biol.* **24**, 809-815. doi:10.1016/j.ceb.2012.10.006
Xiang, K. and Bartel, D. P. (2021). The molecular basis of coupling between poly(A)-tail length and translational efficiency. *eLife* **10**, e66493. doi:10.7554/eLife.66493
Xu, S., Hafer, N., Agunwamba, B. and Schedl, P. (2012). The CPEB protein Orb2 has multiple functions during spermatogenesis in Drosophila melanogaster. *PLoS Genet.* **8**, e1003079. doi:10.1371/journal.pgen.1003079
Zein-Sabatto, H. and Lerit, D. A. (2021). The identification and functional analysis of mRNA localizing to centrosomes. *Front. Cell Dev. Biol.* **9**, 782802. doi:10.3389/fcell.2021.782802
Zimmerman, W. C., Sillibourne, J., Rosa, J. and Doxsey, S. J. (2004). Mitosis-specific anchoring of γ tubulin complexes by pericentrin controls spindle organization and mitotic entry. *Mol. Biol. Cell* **15**, 3642-3657. doi:10.1091/mbc.e03-11-0796

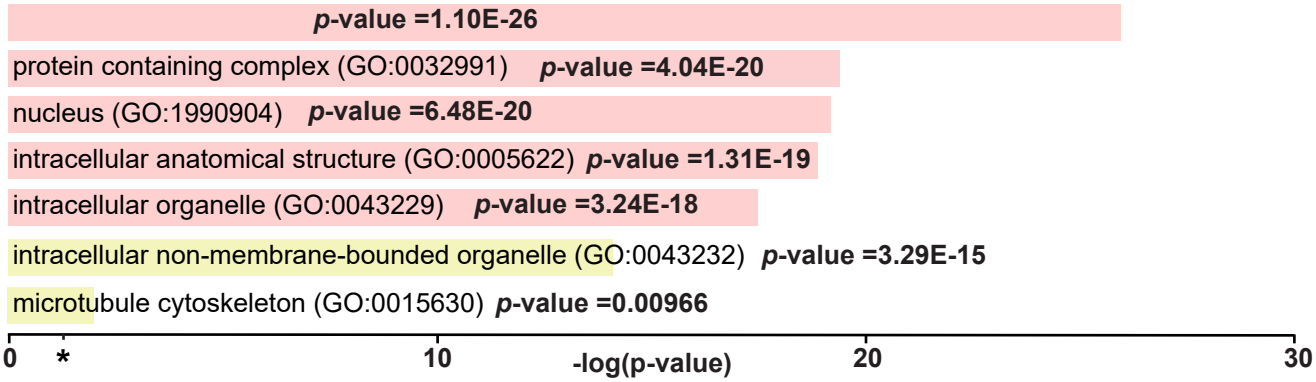

Fig. S1. Common mRNA targets of CPEB1 and Orb

Bar graphs show the top 5 most significant cellular component GO terms (pink) and two centrosome-related components (yellow) identified from common mRNA targets of CPEB1 and Orb. Adjusted *p*-values are displayed; significance cut-off: **p*< 0.05. See Supplemental Table 2 for a list of overlapping mRNA targets from the two centrosome-related terms.

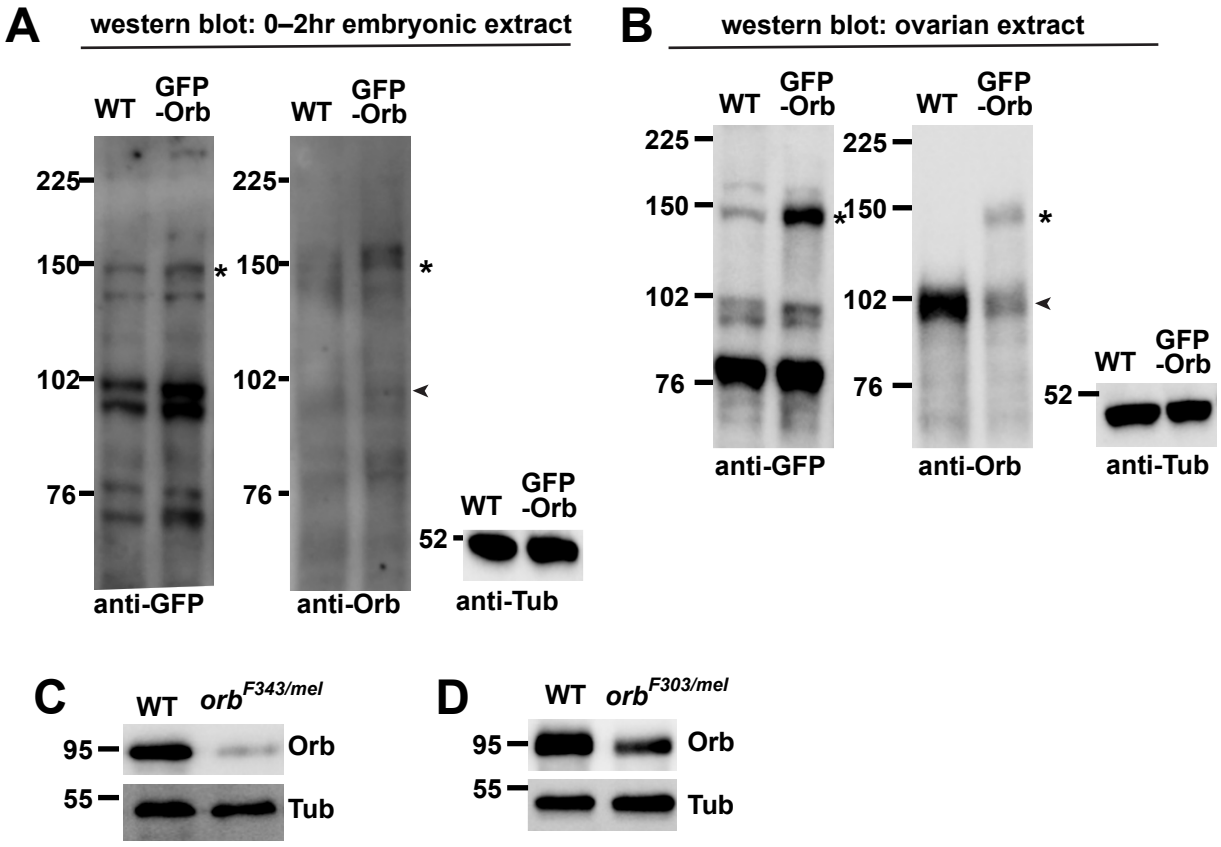

Fig. S2. Orb protein expression in ovaries and embryos

Western blots from (A) 0–2 hr whole embryonic or (B) 2–4 day ovarian extracts from WT or *GFP-Orb*-expressing animals probed with anti-GFP, -Orb, and -β-tubulin antibodies to examine Orb protein expression levels. GFP-Orb is expected to migrate near 150 kDa (asterisks). Endogenous Orb migrates near 102 kDa (arrowhead). (C and D) Immunoblots show Orb protein levels from 2–4 day ovarian extracts from WT versus *orb* transheterozygous mutants. Uncropped blots are available to view on Figshare: https://doi.org/10.6084/m9.figshare.16900429.v4

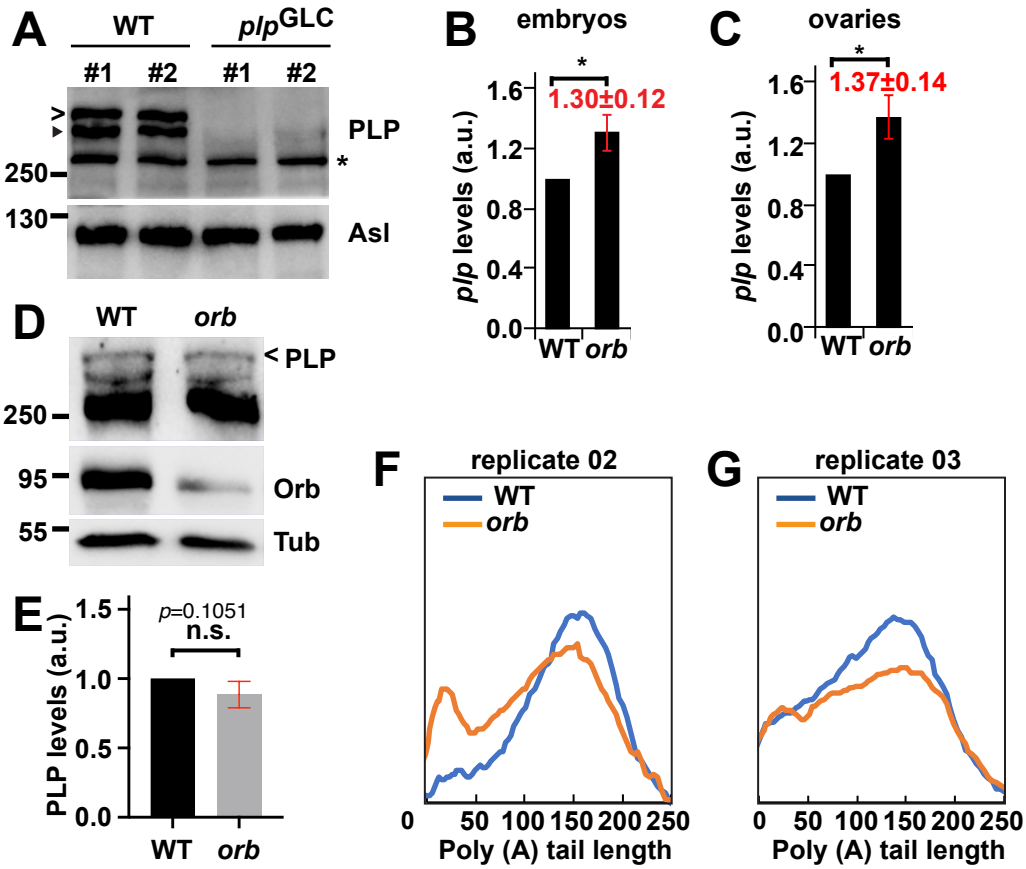

Fig. S3. PLP protein and mRNA expression levels (A) Immunoblots show PLP levels within 1–2 hr WT and *plp* null germline clones (plp^{GLC}) relative to the Asl loading control. Two biological replicates are displayed on the same blot. The upper MW and mid-MW PLP bands are marked by a carrot or arrowhead, respectively, and represent different PLP isoforms. A lower MW band (asterisk) is also detected in the *plp* null extracts and is a non-specific band. Normalized, relative *plp* mRNA levels were examined using qRT-PCR from (B) 0–2 hr embryos or (C) 2–4 day ovarian extracts from WT or orb^{F343}/orb^{mel} mutants. (D) Immunoblots show relative PLP protein levels from 2–4 day ovarian extracts. The upper MW PLP band (carrot) was quantified in (E). (E) Quantification of normalized relative PLP levels from three biological replicates. (F and G) Line profiles from WT vs. orb^{F343}/orb^{mel} PAT products from 0–2 hr embryos from the second and third biological replicates. Poly(A)-tail length was calculated by subtracting the internal PCR product plus G/I tail length from the total PAT product length. Mean ± S.D. are displayed. Significance determined by unpaired t-test; n.s, not significant and *p<0.05. Uncropped blots are available to view on Figshare: https://doi.org/10.6084/m9.figshare.16900429.v4 and https://doi.org/10.6084/m9.figshare.16900471.v4

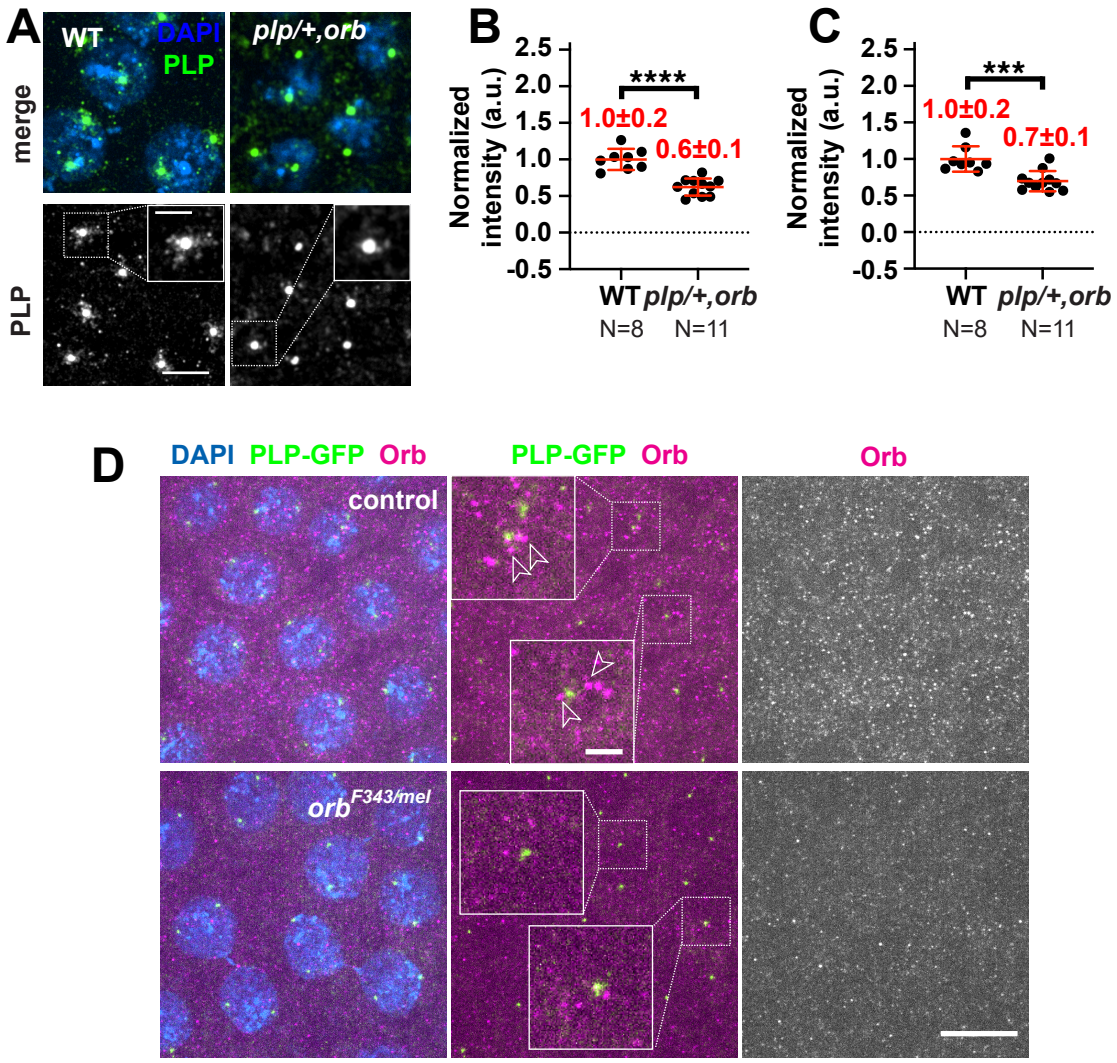

Fig. S4. Localization of PLP and Orb proteins within syncytial embryos

(A) Maximum-intensity projections of NC 13 embryos of WT versus *plp*^{2172}/+, *orb*^{F343}/*orb*^{mel} embryos stained with anti-PLP antibodies (green). Quantifications show results from (B) manual quantification of PLP intensity within 2 µm of the centrosome using Fiji vs. (C) a Python-based pipeline, as described in *Materials and Methods*. Each dot represents the average PLP intensity from 10 centrosomes randomly selected from a single embryo. Mean± S.D. are displayed. ***p<0.001 or ****p<0.0001 by unpaired t-test. (D) Images show maximum intensity projections of NC 12 interphase embryos of control versus *orb*^{F343}/*orb*^{mel} embryos expressing *PLP-GFP* (green) and stained with anti-Orb 6H4 antibodies (magenta) to visualize Orb protein distribution. Open arrowheads mark Orb protein near centrosomes. The same range LUT was used to display Orb signals in both genotypes. Images are representative of N=4 control and N=6 age-matched *orb* mutants. Bars: (A) 5 µm; 2 µm (insets) and (D) 10 µm; 1 µm (insets).

Table S1. Summary of the quantification of RNA localization to centrosomes.

For every image quantified, the following parameters are listed: A) Figure, B) Genotype, C) mRNA analyzed, D) NC stage of embryos, E) cell cycle phase of embryos, F) (n) embryos quantified, G) (n) centrosomes segmented, H) total number (n) of mRNA objects detected, I) all mRNA objects (n) at the centrosome surface, J) total number (n) of single molecules of mRNA after single molecule normalization, and K) number of single molecules of mRNA at the centrosome surface. The values from Column K are displayed in the figures.

Click here to download Table S1

Table S2. Common mRNA targets of CPEB1 and Orb.

Three lists of overlapping mRNA targets shared between Orb and CPEB1 are provided: 1) all common genes, 2) common genes within GO-term 'microtubule cytoskeleton,' and 3) common genes within GO-term 'non-membrane organelle.' *PCNT*/*plp* are highlighted.

Click here to download Table S2

Table S3. Antibodies used for immunofluorescence.

Click here to download Table S3

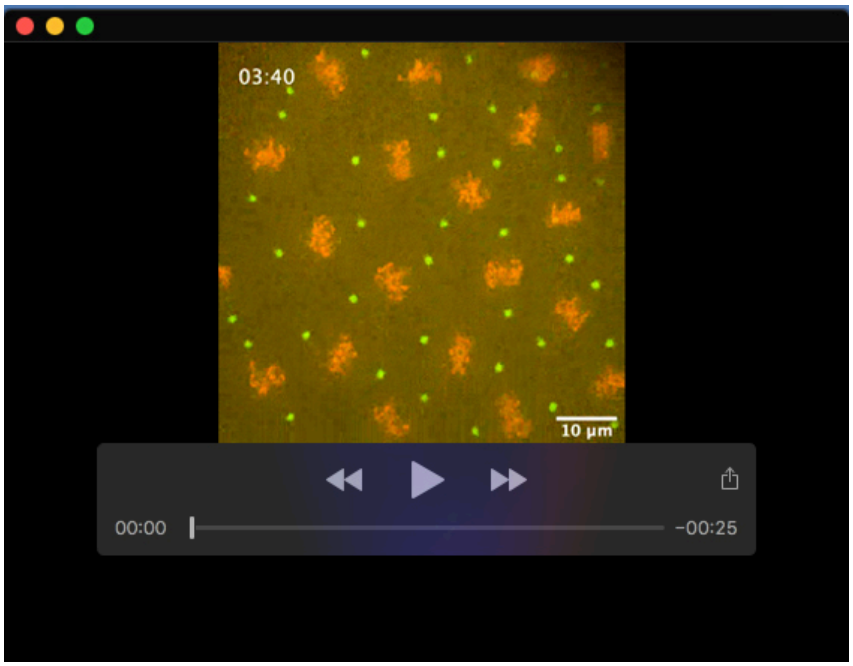

Movie 1. GFP-γTub and H2A-RFP from NC 12 interphase to NC 14 interphase in a control embryo. Live control *Drosophila* embryo expressing *GFP-γTub* (green) and *H2A-RFP* (red). Frames were captured at 20 s intervals over 31 min 40 s using a 1 µm z-step size over 14 µm total depth. Video displayed using a playback speed of 6 FPS (frame per second). Still images are shown in Fig. 8A. Bar: 10 µm.

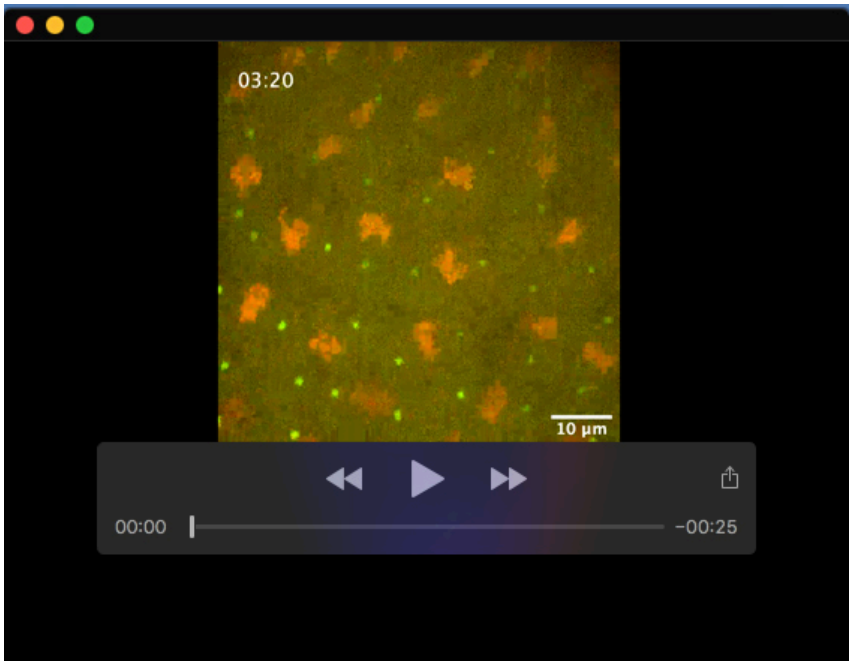

Movie 2. GFP-γTub and H2A-RFP from NC 12 interphase to NC 14 interphase in an *orb* mutant embryo. *Drosophila* embryo expressing *GFP-γTub* (green) and *H2A-RFP* (red). Frames were captured every 20 s for 29 min 40 s using a 1 µm z-step size over 14 µm total depth. Images were captured at 1 µm z-intervals over a 10–15 µm volume at 20 s intervals. Video displayed with a playback speed of 6 FPS. Still images are shown in Fig. 8B. *orb* mutant: orb^{F303}/orb^{mel}. Bar: 10 µm.

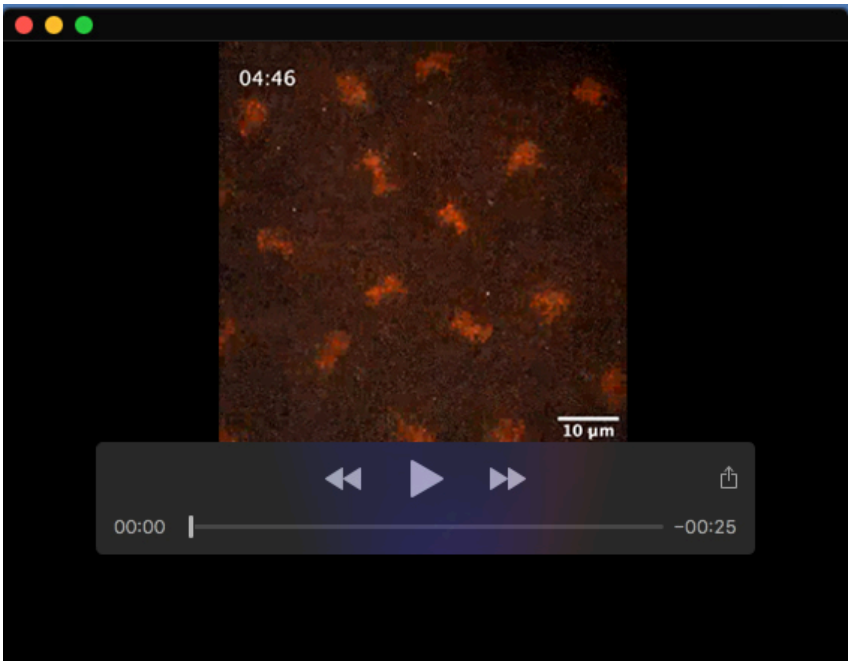

Movie 3. PLP-GFP and H2A-RFP from NC 12 interphase to NC 14 interphase in a *PLP-GFP*; *orb* mutant embryo. *Drosophila* embryo expressing *PLP-PLP* (gray) and *H2A-RFP* (red). Frames were captured every 22 s for 30 min 04 s using a 1 µm z-step size over 15 µm total depth. Video is displayed using a playback speed of 6 FPS. Still images are shown in Fig. 8C. genotype: *PLP-GFP*; orb^{F303}/orb^{mel}. Bar: 10 µm.